Title

Human Polo-like Kinase Inhibitors as Antiplasmodials.

Permalink

https://escholarship.org/uc/item/5563q4jg

Journal

ACS Infectious Diseases, 9(4)

Authors

Bohmer, Monica

Wang, Jinhua

Istvan, Eva

et al.

Publication Date

2023-04-14

DOI

10.1021/acsinfecdis.3c00025

Peer reviewed

Human Polo-like Kinase Inhibitors as Antiplasmodials

Monica J. Bohmer[¶],

Division of Molecular Microbiology, Burnett School of Biomedical Sciences, University of Central Florida, Orlando, Florida 32826, United States;

Jinhua Wang[¶],

Department of Biological Chemistry and Molecular Pharmacology, Harvard Medical School, Boston, Massachusetts 02215, United States;

Department of Cancer Biolo gy, Dana-Farber Cancer Institute, Boston, Massachusetts 02215, United States

Eva S. Istvan,

Division of Infectious Diseases, Department of Medicine and Department of Molecular Microbiology, Washington University School of Medicine, St. Louis, Missouri 63110, United States

Madeline R. Luth,

Department of Pediatrics, School of Medicine, University California, San Diego, La Jolla, California 92093, United States

Jennifer E. Collins,

Division of Molecular Microbiology, Burnett School of Biomedical Sciences, University of Central Florida, Orlando, Florida 32826, United States;

Edward L. Huttlin,

Department of Cell Biology, Harvard Medical School, Boston, Massachusetts 02115, United States;

Lushun Wang,

Department of Chemical and Systems Biology, ChEM-H, Stanford Cancer Institute, School of Medicine, Stanford University, Stanford, California 94305, United States;

Nimisha Mittal,

Corresponding Authors: Elizabeth A. Winzeler – Department of Pediatrics, School of Medicine, University California, San Diego, La Jolla, California 92093, United States; ewinzeler@ucsd.edu, **Nathanael S. Gray** – Department of Chemical and Systems Biology, ChEM-H, Stanford Cancer Institute, School of Medicine, Stanford University, Stanford, California 94305, United States; nsgray01@stanford.edu, **Debopam Chakrabarti** – Division of Molecular Microbiology, Burnett School of Biomedical Sciences, University of Central Florida, Orlando, Florida 32826, United States; dchak@ucf.edu. E.A.W. and N.S.G. are co-corresponding authors.

[¶]M.J.B. and J.W. contributed equally to this paper.

Department of Pediatrics, School of Medicine, University California, San Diego, La Jolla, California 92093, United States

Mingfeng Hao,

Department of Biological Chemistry and Molecular Pharmacology, Harvard Medical School, Boston, Massachusetts 02215, United States;

Department of Cancer Biolo gy, Dana-Farber Cancer Institute, Boston, Massachusetts 02215, United States; Present Address: Affiliations for M.H. and N.P.K. are those in which the research was conducted

Nicholas P. Kwiatkowski,

Department of Biological Chemistry and Molecular Pharmacology, Harvard Medical School, Boston, Massachusetts 02215, United States;

Department of Cancer Biolo gy, Dana-Farber Cancer Institute, Boston, Massachusetts 02215, United States; Present Address: Affiliations for M.H. and N.P.K. are those in which the research was conducted

Steven P. Gygi,

Department of Cell Biology, Harvard Medical School, Boston, Massachusetts 02115, United States;

Ratna Chakrabarti,

Division of Cancer Research, Burnett School of Biomedical Sciences, University of Central Florida, Orlando, Florida 32826, United States

Xianming Deng,

School of Life Sciences, Xiamen University, Xiamen, Fujian 361102, China;

Daniel E. Goldberg,

Division of Infectious Diseases, Department of Medicine and Department of Molecular Microbiology, Washington University School of Medicine, St. Louis, Missouri 63110, United States;

Elizabeth A. Winzeler,

Department of Pediatrics, School of Medicine, University California, San Diego, La Jolla, California 92093, United States;

Nathanael S. Gray,

Department of Chemical and Systems Biology, ChEM-H, Stanford Cancer Institute, School of Medicine, Stanford University, Stanford, California 94305, United States;

Debopam Chakrabarti

Division of Molecular Microbiology, Burnett School of Biomedical Sciences, University of Central Florida, Orlando, Florida 32826, United States;

Abstract

Protein kinases have proven to be a very productive class of therapeutic targets, and over 90 inhibitors are currently in clinical use primarily for the treatment of cancer. Repurposing these inhibitors as antimalarials could provide an accelerated path to drug development. In this study,

we identified BI-2536, a known potent human polo-like kinase 1 inhibitor, with low nanomolar antiplasmodial activity. Screening of additional PLK1 inhibitors revealed further antiplasmodial candidates despite the lack of an obvious orthologue of PLKs in *Plasmodium*. A subset of these inhibitors was profiled for their *in vitro* killing profile, and commonalities between the killing rate and inhibition of nuclear replication were noted. A kinase panel screen identified *Pf*NEK3 as a shared target of these PLK1 inhibitors; however, phosphoproteome analysis confirmed distinct signaling pathways were disrupted by two structurally distinct inhibitors, suggesting *Pf*NEK3 may not be the sole target. Genomic analysis of BI-2536-resistant parasites revealed mutations in genes associated with the starvation-induced stress response, suggesting BI-2536 may also inhibit an aminoacyl-tRNA synthetase.

Graphical Abstract
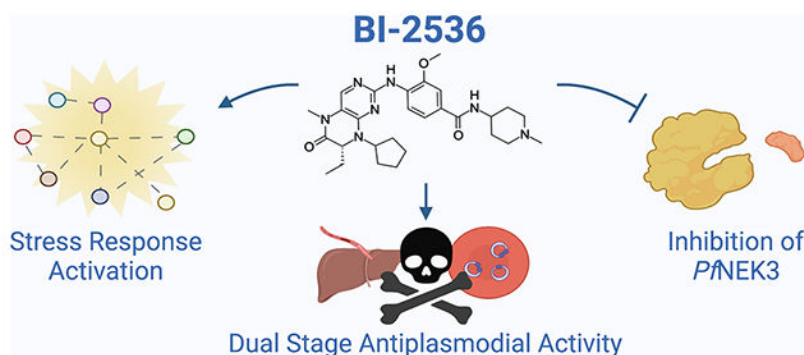
Keywords

malaria; Plasmodium; kinase; PLK; NEK; antiplasmodial; antimalarial

---

Malaria represents a global threat, with ~241 million cases and 627,000 deaths worldwide in 2020.[1] The *Plasmodium* parasite's propensity for developing drug resistance has now extended to frontline treatment with artemisinin combination therapy (ACT); ACT resistance has been detected in both Asia and Africa, accelerating the need for new drugs.[2,3] The most lethal species, *Plasmodium falciparum*, displays a complex life cycle from mosquitoes to host, where parasites mature first in the liver before entering into the symptomatic blood stage and finally advancing to the retransmitted gametocyte stage. Protein kinases are heavily involved in the regulation of each of these stages, making them a desirable target for rational drug design. Additionally, the plasmodial kinome has been found to be highly divergent from the human kinome, which offers the potential for high selectivity.[4] The repurposing of existent kinase inhibitors offers a viable strategy to target these essential enzymes in *Plasmodium* while accelerating the drug development timeline. The dissimilarity between human and plasmodial kinomes presents both challenges and opportunities for repurposing; while it hinders efforts to model plasmodial targets *in silico* based on human orthologues, the pool of available inhibitors has been bolstered by over two decades of kinase inhibitor research, predominantly in the cancer field.[5] Considerable progress has been made toward advancing inhibitor scaffold design, target identification, and off-target mitigation strategies, all of which may be leveraged for antimalarial drug development.

Large-scale screening efforts of kinase inhibitor libraries have already successfully identified compounds active against both blood and liver-stage parasites, further validating this approach.[6]

In the following work, we screened a kinase inhibitor library curated by the Harvard Medical School (HMS) Library of Integrated Network-based Cellular Signatures (LINCS) Center (www.lincsproject.org). The LINCS program is a consortium-based project with the goal of illuminating cellular response pathways by observing the impact of pathway perturbations. The resulting data are publicly made available to assist in the development of therapeutics. From these efforts, nine kinase inhibitors with antiplasmodial activity were identified, including the potent and selective polo-like kinase 1 (PLK1) inhibitor BI-2536.[7] Polo-like kinases (PLKs) are serine/threonine kinases that regulate various components of cell division in mammals; however, no PLKs have currently been identified in *Plasmodium*.[8,9] Exploration of additional PLK1 inhibitors, comprised of both BI-2536 analogues and structurally distinct chemical scaffolds, confirmed that the activity against the human PLK1 enzyme does not correlate with antiplasmodial activity. Furthermore, we identified the plasmodial NIMA (never in mitosis gene A)-related kinase, *Pf*NEK3, as a potential target of BI-2536 and other PLK1 inhibitors. Phosphoproteomic analysis of the two most potent structurally distinct *Pf*NEK3 inhibitors showed little overlap, however, highlighting the complexity of these signaling pathways and the possibility of additional *in vitro* targets. In BI-2536-resistant parasites, we detected a series of mutations in genes related to the starvation-induced stress response. A hallmark of activated stress response, increased eIF2a phosphorylation, was also observed in BI-2536-treated parasites, corroborating involvement in this pathway and underscoring the likelihood of polypharmacology, potentially with an aminoacyl-tRNA synthetase as a secondary target.

RESULTS AND DISCUSSION

Kinase Library Screening Identifies Antiplasmodial Effects of Polo-Like Kinase Inhibitor BI-2536.

To identify kinase inhibitors with antiplasmodial potential, we performed a fixed concentration screen of 201 compounds from the HMS LINCS library against the multidrug-resistant *Plasmodium falciparum* strain Dd2. We observed a range of inhibition at 1μM, with the majority of compounds showing <30% inhibition and an overall hit rate of 4.5% (Figure S1). Of the inhibitors tested, nine exhibited >90% inhibition, prompting their EC$_{50}$ determination (Table S1). Reflecting the diversity within the compound library, these inhibitors were associated with a variety of human targets, including Akt1, PI3K, PI4K, HSP90, and mTOR. The most potent compound, torin2 (Dd2 EC$_{50}$ =5.30 ± 0.30 nM), has been previously explored as an antimalarial.[10] Similarly, the HSP90 inhibitor NVPAUY922,[11] the c-Met inhibitors Crizotinib and PHA665752,[12] the AKT inhibitor A443654,[13] and the PI3K/PI4K inhibitors INK128, PIK-93, and GSK2126458[14] have all been evaluated in *Plasmodium*. However, the potent PLK1 inhibitor BI-2536 (hereafter compound **1**) displayed a low nanomolar activity in Dd2 (EC$_{50}$ = 178 ± 12 nM) and had, to our knowledge, not yet been characterized as an antiplasmodial compound. We therefore chose to pursue this compound for further investigation.

Antiplasmodial Activity Has Little Correlation with the Human PLK1 Activity.

Along with other members of the Apicomplexa phylum, *Plasmodium* parasites appear to lack polo-like kinases.[8] To probe the potential relationship between human PLK1 inhibition and antiplasmodial activity of compound **1**, we utilized a previously synthesized set of compound **1** analogues with either 7,8-dihydropteridinone (compounds **2**–**6**) or related pyrimido-diazepine (compounds **7**–**10**) core, and various substitution groups were tested for both cellular antiplasmodial activity and human PLK1 enzymatic activity.[15] We evaluated the antiplasmodial activity in both the Dd2 strain and the chloroquine-sensitive strain 3D7, shown in Table 1. Interestingly, there was considerable variation in antiplasmodial activity among these compounds regardless of scaffold, with some inhibitors showing no *in vitro* activity at the highest concentrations tested (5 μM). It is of interest to note that compound **2** while exhibiting good antiplasmodial activity was inactive against PLK1. Presumably, the lack of cytotoxicity could be attributed to the loss of PLK1 activity of this compound.

Having discovered the antiplasmodial activity of human PLK1 inhibitors, we focused our attention on additional PLK1 inhibitors. We compiled a set of seven commercially available PLK1 inhibitors: BI-6727, a close analogue of BI-2536 (compound **11**), GSK461364 (compound **12**), MLN0905 (compound **13**), SBE 13 (compound **14**), NMS-P937 (compound **15**), ON-01910 (compound **16**), and GW843682 (compound **17**). While these compounds are all very potent PLK1 inhibitors, displaying IC_{50} values under 9.0 nM, only two compounds demonstrated nanomolar antimalarial potency—compounds **11** and **12** (Table 2). Additionally, we evaluated a set of six potent PLK1 inhibitor analogues derived from a 2,4-diarylaminopyrimidine scaffold provided by the Deng Laboratory at Xiamen University (compounds **18**–**23**).[16] Among these compounds, antiplasmodial potencies varied, with Dd2 EC_{50} values ranging from 336 nM to 2.78 μM (Table 2). In general, the antiplasmodial activity varied widely among both compound **1** structural analogues and the known PLK1 inhibitors, as reflected in the broad range of EC_{50} values observed. Of all of the compounds tested, compound **1** displayed the most potent antiplasmodial activity followed by its close analogue compound **11** (Dd2 EC_{50}= 230 ± 14 nM). Compound **2** although being less active against *Plasmodium* exhibited the highest selectivity (Table 1). Of the inhibitors screened in both the Dd2 and 3D7 parasite lines, no noteworthy difference in activity was noted, with resistance indices (RI) ranging from 0.34 to 1.5. Additionally, evaluation in clinical isolates displaying artemisinin and piperaquine resistance demonstrated that hit compounds such as compound **1** maintain potency (Table S2).

To assess the therapeutic potential of these compounds, we also evaluated growth inhibition in the human hepatocarcinoma line, HepG2. We found that these compounds displayed a range of cytotoxicity, with HepG2 EC_{50} values from 1.87 μM to greater than 25 μM and parasite over human selectivity ranging from 1- to 58-fold (Tables 1 and 2). The most active inhibitor, compound **1**, showed a selectivity index (SI) of 21 (HepG2 EC_{50} = 3730 ± 520 nM), making it the second most selective of the inhibitors tested. Based on the *in vitro* activity, there appeared to be no positive correlation between PLK1 inhibition and antiplasmodial potency. This finding was validated through a two-tailed regression coefficient *t*-test, which confirmed no significant correlation (Figure 1A).However, there was a positive correlation ($p < 0.0001$) between cytotoxicity and PLK1 inhibition among

compound **1** structural analogues, but this was not observed among the diverse PLK1 inhibitors (Figure S2). A relationship was not seen between cytotoxicity and inhibition in Dd2 in compound **1** structural analogues (Figure 1B), and while the correlation among PLK1 inhibitors is significant ($p = 0.0104$), there appears to be an additional source of variation, supporting the separation between antiplasmodial potency and host-cell activity. These findings also suggest that selectivity could theoretically be improved by reducing affinity for PLK1 without sacrificing parasite inhibition.

PLK1 Inhibitors Show a Moderate Killing Profile with Early Life Cycle Arrest.

To further characterize the antiplasmodial impact of these PLK1 inhibitors, we assessed their killing profile in Dd2. Included in the assay were compound **1**, its close analogue, compound **11**, and compound **12**, which has a distinct structure. Dd2 cultures were treated with $10 \times EC_{50}$ of compound or vehicle control for 12, 24, or 48 h before removal. Cultures were then monitored for up to 96 h, or two asexual life cycles. Every 24 h, cultures were evaluated for parasite survival by flow cytometry with SYBR Green I and MitoTracker Deep Red FM staining to monitor the levels of viable parasites over time. Killing profiles were compared to the vehicle, to a slow-acting compound, atovaquone, and to a fast-acting compound, dihydroartemisinin (DHA). As shown in Figure 2A, all three inhibitors had an initial impact to parasitemia after 12 h of exposure. Parasites treated with compound **1** and compound **12** began to recover after 72 h, while compound **11** treated parasites showed a shorter time to recovery, around 48 h. After 24 h of treatment, parasites treated with compound **11** and compound **12** showed marked improvement at 72 and 96 h, respectively, and compound **1** treated parasites remaining more in line with fast-acting DHA, failing to recover within 4 days (Figure 2B). Upon 48 h of compound exposure, all cultures exposed to the PLK1 inhibitors remained under 1% parasitemia for the duration of the assay (Figure 2C). These results suggest that while compound **1** kills more rapidly than compound **11** or compound **12**, all three compounds show a moderate killing profile, with 24–48 h of compound incubation required for a full killing effect.

We next sought to determine the stage at which these inhibitors exert their antiplasmodial effects. To accomplish this, synchronized Dd2 parasites were treated at the early ring (6 HPI), late ring (18 HPI), late trophozoite (30 HPI), and schizont (42 HPI) stages with $5 \times EC_{50}$ of compound **1**, **11**, or **12**. Samples were collected for flow cytometry and Giemsa staining every 12 h until reinvasion and signs of new rings (~54 HPI). When applied during the early ring stage (Figure 3), all three compounds appeared to induce arrest prior to DNA replication based on YOYO-1 staining, although a clear increase in size was noted from ring onward (Figure S3). A similar phenotype was observed when these inhibitors were applied later in the ring stage. However, compound **11** treated parasites showed a delayed increase in the YOYO-1 signal at 54 h, indicating some parasites were able to begin DNA replication. With a 30 HPI addition of compound, parasites treated with all compounds showed signs of entering into schizogony, reflected by an increase in both total DNA content and DNA content per cell at 42 HPI. When applied after schizogony, the effect was much less pronounced, and an increase in DNA content for all compounds was detected, albeit less noticeably for compound **12**. Together, this suggests the PLK1 inhibitors have a shared impact on DNA replication when added early in the life cycle.

Having characterized the effect of compound **1** in the plasmodial intraerythrocytic stage, we performed a liver-stage assay to assess compound activity against parasite infection of hepatocytes. HepG2 were pretreated with a serial dilution of compound **1** for 18 h and subsequently infected with luciferase-expressing *Plasmodium berghei* sporozoites. After 48 h, viable exoerythrocytic parasites, indicative of successful establishment of liver-stage infection, were quantified via bioluminescence. We found that compound **1** displayed nanomolar liver-stage activity, with an EC_{50} of 367 ± 52 nM (Figure S4), though further investigation would be necessary to confirm that this activity extends to human malaria. Potent activity in both liver and intraerythrocytic stages is a particularly desirable trait in developing antimalarials as these compounds can impart both prophylactic and therapeutic effects.

PLK1 Inhibitors Exhibit Plasmodial Kinase PfNEK3 Inhibition.

Given the similarities between the *in vitro* profile of the PLK1 inhibitors tested and the lack of apparent correlation with PLK1 activity, we attempted to probe for other possible antiplasmodial protein kinase targets. As *Plasmodium* lacks polo-like kinases, we began by employing a kinase panel screening assay that utilizes a three-hybrid split-luciferase competitive binding assay[17] utilizing a panel of 11 *in vitro* translated plasmodial kinases. With this assay, we evaluated six of the most potent PLK1 inhibitors identified at a fixed 2.5 μM concentration. We noted that one commonality observed in all compounds was the strong inhibition of *Pf*NEK3 (PF3D7_1201600), a plasmodial NIMA (never in mitosis gene A)-related kinase (NEK) (Table 3). Compound **1** exhibited the greatest inhibition, with only 4.7% enzyme activity remaining, followed by compound **12** with 9.7%. Of the analogues with the 7,8-dihydropteridinone core, compound **11** retained strong *Pf*NEK3 inhibition (11.1% activity remaining) yet was less selective than compound **1**, while compound **2** displayed the most pan-kinase inhibition, as well as markedly reduced *Pf*NEK3 inhibition (39.6% activity remaining). The two 2,4-diarylaminopyrimidine compounds **18** and **19** demonstrated pan-kinase inhibition with a similar pattern in addition to notable *Pf*NEK3 inhibition with just 15.4 and 18.5% activity remaining, respectively. All targets with percent activity remaining lower than 40% were tested for IC_{50} using the same assay; these values are shown in nanomolars in parentheses in Table 3.

Interestingly, while compounds **1** and **12** are touted for their PLK1 inhibitory potency, both compounds have been shown to inhibit multiple human NEKs among their off targets in the KINOMEscan competitive binding assay, with compound **12** displaying more broad activity (NEK1 K_d = 1.8 μM, NEK2 K_d = 260 nM, NEK5 K_d = 1.1 μM, NEK9 K_d = 1.1 μM) than compound **1** (NEK2 K_d = 2.0 μM, NEK3 K_d = 720 nM, NEK7 K_d = 6.1 μM).[18] In humans, there are 11 NEK paralogues involved in the cell cycle though *P. falciparum* contains only four (*Pf*NEK1–4). *Pf*NEK1 (PF3D7_1228300) is essential to the asexual blood stage and is expressed in male gametocytes.[19] *Pf*NEK2 (PF3D7_0525900) is implicated in the sexual stage of the parasite, particularly the development of the plasmodial zygote, the ookinete.[20] *Pf*NEK4 (PF3D7_0719200), while not essential for schizogony or gametocytogenesis, is associated with sexual commitment.[21] *Pf*NEK3 had been shown to be expressed late in the asexual blood stage and in gametocytes; however, it is believed to be nonessential for *P. falciparum* asexual stage development and instead

plays a larger role in gametogenesis.[22–24] *Pf*NEK3 is unusual when compared to other plasmodial NEKs and human NEKs. A homology search with protein–protein BLAST (https://blast.ncbi.nlm.nih.gov/) reveals that the kinase domain of *Pf*NEK3 is most similar to human NEK9, though only at 35% identity. Additionally, the highly conserved glycine-rich loop (GxGxxG) in the ATP-binding site is completely absent in *Pf*NEK3.[22] *Pf*NEK3 displays a dual kinase function, autophosphorylating serine, threonine, and tyrosine residues, with the tyrosine autophosphorylation playing the largest role in the modulating activity.[25] *Pf*NEK3 has been demonstrated to phosphorylate *Pf*MAP2 (PF3D7_1113900) *in vitro*, in addition to myelin basic protein (MBP), a commonly used substrate for experimental kinase assays.[22] The exact roles of *Pf*NEK3 and *Pf*MAP2 in relation to a broader phosphosignaling cascade is unknown, and inferences based on eukaryotic MAPK pathway provided limited insight as *Plasmodium* lacks the canonical MAPK signaling module.[26] However, the fact that *Pf*NEK3 does phosphorylate *Pf*MAP2 highlights the variability in *Pf*NEK3 functionality and hints at roles aside from mitosis. If the inhibition of *Pf*NEK3 is to some degree responsible for antiplasmodial activity, these other roles may be more influential, as *Pf*MAP2 appears not to be essential to the asexual stage.[27] Aside from potential therapeutic applications, the discovery of selective inhibitors of *Pf*NEK3 may also allow chemical interrogation of this atypical kinase and deepen the understanding of the plasmodial kinome.

Along with NEKs, Aurora-related kinases (ARKs) also play an essential role in the regulation of the plasmodial life cycle.[29] Furthermore, it has been reported that mutations in either *Pf*NEK1 or *Pf*ARK1 confer resistance to a human Aurora kinase inhibitor, suggesting a relationship between the two kinases.[28] Due to the potential biological connection between *Pf*NEKs and Aurora-related kinases (ARKs), compounds **1** and **12** were also tested against the three known *Pf*ARKs.[29] *Pf*ARK1 and *Pf*ARK3 were included in the KinaseSeeker assay, and no significant inhibition was seen (Table 3). Activity against *Pf*ARK2, found to be essential to the asexual blood stage, was assessed with a radioactive kinase assay (Figure S5A); however, neither compound displayed inhibitory effects in *Pf*ARK2 at the highest concentrations tested (2 μM).[24] An ADP-Glo assay confirmed this lack of activity in both *Pf*ARK2 and the human Aurora kinase, AurA, up to 5 μM (Figure S5B).

To confirm the split-luciferase assay results, a radioactive kinase assay was performed with purified recombinant *Pf*NEK3 and MBP as a substrate. When assessed at a concentration up to 2 μM, the analogues with the greatest antiplasmodial potency, compounds **1** and **12**, showed a clear dose-dependent response to *Pf*NEK3 phosphorylation (Figure S6). We then evaluated a subset of compound **1** structural analogues, representing a range of antiplasmodial potencies, at a fixed 1 μM using the same assay (Figure 4A). As shown in Figure 4B, compound **1** and two analogues with the 7,8-dihydropteridinone core, compounds **3** and **4**, inhibited *Pf*NEK3 more strongly than the pan-kinase inhibitor staurosporine. When the percent of *Pf*NEK3 activity remaining is plotted against the Dd2 EC_{50}, only 6/8 of the analogues show a correlation between enzyme inhibition and *in vitro* inhibition, and compounds **3** and **4** appear as outliers (Figure 4C). This persisted when the *Pf*NEK3 IC_{50} was determined using the same assay, with a significant correlation calculated for 7/8 compounds tested only when values for compound **4** were removed (Table S3).

Given these findings, the inhibition of PfNEK3 is unlikely the sole predictor of *in vitro* inhibition for these repurposed PLK1 inhibitors. Some of the compounds, such as compound **4**, may show a greater proclivity for other targets in a whole cell environment. Furthermore, considering the nonessentiality of PfNEK3 to the asexual blood stage, there are likely alternate or additional targets.

Compound **1** is known to potently inhibit the human bromodomain-containing protein BRD4 in addition to PLK1.[30,31] In fact, along with tubulin, bromodomains are common nonkinase targets of kinase inhibitors.[32] In 2016, an open access data set was released by the Structural Genomics Consortium (SGC) that contained the crystal structure of compound **1** cocrystalized with PfBDP4 (PDB ID: 4PY6) and explored the antiplasmodial effects and binding kinetics.[33] They identified the PfBP4 K_d for compound **1** to be ~100 nM, and the 3D7 EC_{50} recorded was comparable to our findings (~200 nM).[33] The aforementioned crystal structure was later the basis of an *in silico* docking-based screen of compounds with the bromodomains of PfBDP1 and PfGCN5.[34] However, when tested *in vitro* with Dd2 culture, the antiplasmodial effects were modest, with the most potent compound demonstrating an IC_{50} of 3.2 μM.[34] The additional target of a bromodomain alongside PfNEK3 is intriguing, as bromodomain protein inhibitors are under consideration as emerging antimalarials.[35]

In Vitro Evolution of Resistance for Target Identification.

In addition to kinase panel screening, we also sought to identify a target through the creation of parasite lines resistant to compound **1**. With increased drug pressure applied over ~8 months, resistant parasites were generated in the *P.falciparum* strains Dd2, 3D7, and Dd2-Polδ, a strain with a DNA polymerase δ mutation that confers hypermutability (Figure 5A).[36] Whole genome sequencing (WGS) was conducted with Dd2 and 3D7 selections. Clonal parasites were obtained from two independent Dd2-Polδ selections, and two clones from each were sequenced: AE9, AG8, BB5, and BE11. Sequencing revealed that, compared to the respective parental strain, resistant parasites from all selections in 3D7 possessed single nucleotide polymorphisms (SNPs) in PfMDR1 (PF3D7_0523000), an ATP-binding cassette transporter implicated in resistance to multiple antimalarial drugs,[37] and amplification of transporter PfABCI3 (PF3D7_0319700), which has also been associated with resistance to numerous antiplasmodial scaffolds (Supporting Files 1 and 2).[38] Among resistant Dd2 cultures, SNPs within PfMDR1 were observed in two of the three selections. In most Dd2-Polδ clones, PfMDR1 amplification was noted, though BB5 lacked this feature. Interestingly, all four of the Dd2-Polδ clones possessed SNP-induced missense mutations in genes associated with the starvation-induced stress response. In both AE9 and AG8, there were mutations in the methionyl-tRNA synthetase PfMRS[api] (PF3D7_1005000), the autophagy-related E1 activating enzyme PfATG7 (PF3D7_1126100), and an eIF2α kinase, PfPK4 (PF3D7_0628200). BE11 possessed a mutation in PfVPS15 (PF3D7_0823000), a kinase that assists in early autophagosome assembly, while BB5 contains a mutation in PfSYN17 (PF3D7_0210700), a homologue of syntaxin 17 that facilitates fusion of the autophagosome to the lysosome.[39] The prevalence of mutations in genes involved in tRNA maturation and aminoacylation and in the starvation response suggested that an additional target of compound **1** may be an aminoacyl-tRNA synthetase (aaRS).

To determine whether compound **1** does indeed activate the stress response pathway, we investigated increases in eIF2α phosphorylation as an indicator of an activated stress response. The eIF2α subunit plays an important role in post-transcriptional control of protein expression; phosphorylation prohibits the recycling of eIF2α-GDP to eIF2α-GTP, leading to the inability to form the ternary complex, a component of the preinitiation complex, and to a global reduction of translation and a prioritization of translation of stress response-related proteins.[40] In vertebrate cells, four kinases are capable of phosphorylating eIF2α, each responding to a different cellular stressor.[40] In *Plasmodium*, eIF2α phosphorylation is conducted by three kinases, *Pf*eIK1 (PF3D7_1444500), *Pf*eIK2 (PF3D7_0107600), and *Pf*PK4 (PF3D7_0628200), the latter of which is essential to the asexual life cycle.[41–43] To evaluate the effect of compound **1** on eIF2α phosphorylation, Dd2 cultures in the primarily late ring stage were treated for 3 h at three concentrations: 10, 1, and 0.1 μM. Two known antiplasmodial compounds served as controls for eIF2α phosphorylation; borrelidin, a threonyl-tRNA synthetase inhibitor,[44] and halofuginone, a prolyl-tRNA synthetase inhibitor,[45] were used at 200 nM each. Western blot analysis revealed that phosphorylation of eIF2α was notably increased upon compound **1** treatment, though not to the extent caused by treatment with the confirmed aaRS inhibitors, despite the high concentration of compound used (Figure 5B). Since eIF2α phosphorylation can result from activation of disparate stress response pathways, the upstream target of compound **1** eliciting the stress response may be difficult to identify. Since the observed missense mutation in *Pf*MRS[api] alters a conserved residue in one of the enzyme's two methionyl/ leucyl-tRNA synthetase domains (InterPro entry: IPR015413) (Figure 5C), it becomes an intriguing potential target, in addition to *Pf*NEK3, though further investigation is needed.

PLK1 Inhibitors Compound 1 and Compound 12 Show Divergent Phosphoproteomes.

To explore the signaling pathways disrupted by these inhibitors, we performed a comparative phosphoproteomics evaluation. Asynchronous intraerythrocytic Dd2 cultures were incubated for 3 h with 5 $\times$EC$_{50}$ of compound **1**, compound **12**, or DMSO as a control. The protein lysate was digested with LysC and trypsin and labeled with isobaric tandem mass tags (TMTpro)[46] as a 16-plex assay with two other compounds in biological triplicate, as well as a single replicate with a fifth compound; however, these compounds originate from a separate library and will be discussed further in subsequent publications. To quantify proteins and phosphorylation sites, peptides underwent IMAC enrichment to separate phosphorylated and nonphosphorylated peptides before analyzing both peptide populations via quantitative mass spectrometry for comparison to *Plasmodium* and human databases. The analysis of nonphosphorylated peptides resulted in identification of 3515 unique *Plasmodium* proteins, all supported by two or more distinct peptides. While a small number of human proteins were observed, all were single-peptide identifications and were thus discarded. The analysis of the phospho-enriched eluate resulted in the identification of 1593 unique phosphorylation sites; 1494 were identified from *P. falciparum* and 99 from *Homo sapiens* (Table S4). Differential expression compared to the corresponding control was determined for both proteins and phosphosites. The most differential proteins/ phosphosites were ranked by ratio-based paired *Z*-score, and the top 10% were examined further. The full list of detected proteins with more than one peptide and phosphosites can be found in Supporting Files 3 and 4, and the top differential proteins are detailed in Tables

S5 and S6. As seen in Figure 6A and B, when comparing the top differentially expressed phosphosites ($|\log 2(fc)| > 0.585$), there was limited consensus between compounds **1** and **12**, though both compounds induce more extensive downregulation of phosphorylation than upregulation (Tables S7 and S8). Despite differences, there were still several downregulated phosphosites shared between the two treatment conditions, including *Pf* HECT1 site S9833 (PF3D7_0628100), DCP1 site S765 (PF3D7_1032100), *Pf*PAIP1 site S390 (PF3D7_1107300), and *Pf*BTP2 (PF3D7_0704100) site S912.

To view these differential phosphorylation sites in a network context, we identified those proteins bearing one or more of the 10% most differential phosphorylation sites and extracted their corresponding subnetwork from the STRING database (Figure 7A).[47] *Pf* NEK3 was included as well to visualize its connection to the network. Two clusters appear, one containing *Pf*HECT1, *Pf*BTP2, and *Pf*KIC8, and another containing *Pf* PAIP1. *Pf*HECT (PF3D7_0628100), downregulated at site S9833 upon treatment with both compounds, is a HECT family E3 ubiquitin ligase linked to the plasmodial phosphorylation network through direct regulation by *Pf*PP1 (PF3D7_1414400), a phosphatase involved in erythrocyte development and egress.[48] *Pf*BTP2 (PF3D7_0704100), basal complex transmembrane protein 2, has been implicated in late stages of blood stage schizogony, specifically the formation of the basal complex that mitigates cytokinesis, and its phosphorylation is also downregulated by both compounds at site S912.[49] Interestingly, phosphorylation of *Pf*KIC8 (PF3D7_1014900), a speculated Kelch13 interaction partner,[50] was upregulated at site S1500 in the presence of compound **1** but downregulated at site S104 by exposure to compound **12**. *Pf*PAIP1 (PF3D7_1107300), central to the other observed cluster, was also downregulated at site S390 by both compounds. *Pf* PAIP1 is a putative polyadenylate-binding protein-interacting protein thought to facilitate translation by mediating interaction of translational machinery components, specifically RNA helicase eIF4A and polyadenylate-binding proteins.[51] Similarly, phosphorylation of *Pf*DCP1 (PF3D7_1032100) at site S765 is downregulated by both compounds. Like *Pf*PAIP1, *Pf*DCP1 is also involved in translation regulation, as it is a subunit of an m^7G 5′ decapping enzyme that facilitates mRNA decay.[52] Finally, an uncharacterized protein, PF3D7_1036900, was downregulated upon treatment at two sites; treatment with compound **1** led to decreased phosphorylation at site T1037, while compound **12** decreased phosphorylation at both site T1037 and site S805. While the function of this protein is unknown, immunoprecipitation experiments suggest association with the *N*6-adenosine-methyltransferase MT-A70, which plays a role in post-transcriptional control by influencing mRNA stability.[53]

To better assess the similarities and differences between the exposure to compounds **1** and **12**, GO enrichment analysis was performed via PlasmoDB (https://plasmodb.org)[54] using the gene identifiers of the proteins bearing the top differential phosphosites as the foreground data set and the *P. falciparum* 3D7 genome as the background. Terms from top differentially phosphorylated proteins were grouped into simplified categories based on commonalities (Figure 7B–D). We found that both treatments shared biological process terms related to RNA decapping, while compound **1** was enriched in transport as well (Figure 7B). Shared cellular component terms were related to the basal component and

eukaryotic initiation factor 4F (eIF4F) (Figure 7C), and compound **1** was enriched in terms related to the P-body and RNA *N*6-methyladenosine methyltransferase complex, both of which are involved in translational regulation. Shared molecular function terms were related to mRNA binding (Figure 7D). Taken together, while there are similarities to be found between the interactomes of these two inhibitors, it is clear that in addition to *Pf*NEK3, they likely affect disparate signaling pathways. Compound **1** in particular impacts processes related to translational regulation and repression, consistent with downstream effects of the observed eIF2α phosphorylation.

CONCLUSIONS

In this paper, we screened a series of human kinase inhibitors for potential drug repurposing to discover malaria therapeutics. This effort identified compound **1**, a potent inhibitor of the human kinase PLK1. As *P. falciparum* lacks polo-like kinases, we explored compound **1**, structural analogues of compound **1** possessing either a 7,8-dihydropteridinone or a pyrimido-diazepine core, and other PLK1 inhibitors for a potential antiplasmodial mechanism. Through these efforts, we found a majority of the PLK1 inhibitors tested displayed inhibition against the plasmodial homologue of NEK3. For some of the inhibitors, the relationship between *Pf*NEK3 inhibition and antiplasmodial potency was more complex, suggesting additional causative targets. When evaluating the effect of these PLK1 inhibitors *in vitro*, we found that they exerted their greatest effect early in the asexual life cycle; if applied in ring or early trophozoite stages, they appear to affect DNA replication. Additionally, the compounds displayed a moderate killing profile, in general, requiring 24–48 h for a full killing effect. As a probative look at the *in vivo* activity of compound **1**, we treated mice with 50 mg/kg for 4 days. The treatment was found to be inconclusive, and additional work in needed (Figure S7). However, caution is warranted when using *P. berghei* models: while the murine-infective strain is a useful tool, there are some genes that have been reported to be essential in *P. berghei* and dispensable in *P. falciparum* or *vice versa*, and NEK3 is one such example. While NEK3 is essential for schizogony in *P. berghei*, it appears to be refractory in *P. falciparum*.[23,55] This is certainly something to keep in mind when evaluating data from models using *P. berghei*.

The connection between PLKs and NEKs has been well-established in eukaryotic cells, where mitosis is a coordinated effort utilizing PLKs, Aurora kinase, cyclin-dependent kinases, and NEKs. These mitotic kinases are all involved in the duplication, maturation, and separation of centrosomes through the cell cycle.[56] In addition to its function in centrosomal coordination, PLK1 regulates entry from G2 into mitosis, chromosome segregation, cytokinesis, and ciliary assembly.[57] Since *Plasmodium* lacks PLKs, the question arises which kinase (or kinases) executes these functions instead. It has been noted that the paucity of cell-cycle-related kinases in *Plasmodium* suggests that these kinases perform multiple functions, perhaps also as cell cycle checkpoints.[58] *Pf*NEK3 possesses an N-terminal hydrophobic region, which has been omitted when generating recombinant proteins due to issues it poses in solubility.[22] The region is also suspected to contain a localization signal and a transmembrane portion.[22,59] Perhaps this region is involved in anchoring to the nuclear membrane, facilitating proximity to the centriolar plaques, the centrosomal equivalent in *Plasmodium* that likely exerts local control of cell division.[60] It is intriguing to

consider whether *Pf*NEK3 is a kinase involved in the localized control of nuclear division in schizogony as part of a complex, perhaps with other cell cycle kinases. In lieu of PLK1, it is possible that *Pf*NEK3 may fulfill some of the cell cycle duties.

While *Pf*NEK3 can be inhibited *in situ* by these PLK1 inhibitors, a full deconvolution of their mechanism of action would require further efforts, and the possibility of action via inhibition of a host kinase cannot be excluded. Targeting multiple kinases can in fact be desirable as it raises the hurdle for resistance and increase efficacy, though promiscuity must be balanced to mitigate off-target effects.[61] In addition to kinase targets, certain PLK1 inhibitors like compound **1** may also target aaRSs, triggering the cell to initiate a starvation-induced stress response. Since *Plasmodium* possesses aaRSs that reside in the apicoplast, a parasite-exclusive organelle, there is a great potential for development of selectivity, and plasmodial aaRSs have been validated as targets for innovative antimalarial compounds with unique mechanisms of action.[62,63] In fact, repurposing human kinase inhibitors that target plasmodial aaRSs has been recently explored as a source of novel antimalarials.[64] Overall, the results of this study indicate that kinase inhibitors designed to target human PLK1 have potential as antimalarials and as *Pf*NEK3 probes. Since little of the function of *Pf*NEK3 has been elucidated, compound **1** and other such PLK1 inhibitors may be used to interrogate the role of *Pf*NEK3 in the life cycle of *Plasmodium*, in addition to being a chemical starting point for antiplasmodial medicinal chemistry efforts.

METHODS

Chemistry.

Unless otherwise noted, reagents and solvents were obtained from commercial suppliers and were used without further purification. ^{1}H NMR spectra were recorded on a 500 MHz NMR (Bruker-500), and chemical shifts are reported in parts per million (ppm, δ) downfield from tetramethylsilane (TMS). Coupling constants (J) are reported in Hz. Spin multiplicities are described as s (singlet), d (doublet), t (triplet), and m (multiplet). Mass spectra were obtained on a Waters Micromass ZQ instrument (Milford, MA). Preparative high-performance liquid chromatography (HPLC) was performed on a Waters Symmetry C18 column (19 mm × 50 mm, 5 μM) using a gradient of 5–95% methanol in water containing 0.05% trifluoacetic acid (TFA) over 8 min (10 min run time) at a flow rate of 30 mL/min. Purities of assayed compounds were in all cases greater than 95%, as determined by LC-MS analysis. Detailed compound characterization was given in the Supporting Information. Structure graphics were generated by ChemDraw 21.0.0.

Culture Conditions.

P. falciparum Dd2 and 3D7 parasites were cultured with an adapted Trager and Jansen protocol.[65] Cultures were maintained at 37 °C in 5% CO_2 or in 95% N_2/5% CO_2 in RPMI 1640 medium (25 mM HEPES, 26 mM sodium bicarbonate, 15 mg/L hypoxanthine, 25 mg/L gentamycin, 2% dextrose), 0.5% AlbuMAX II (Thermo Fisher, Waltham, MA), and L-glutamine as needed. Human A+ erythrocytes were used to maintain 4% hematocrit. HepG2 human hepatocytes were maintained at 37 °C in 5% CO_2 in Eagle's Minimal Essential

Medium supplemented with 10% fetal bovine serum and 1% antibiotic–antimycotic solution (Gemini Bio, West Sacramento, CA).

SYBR Green I Proliferation Assay.

This assay was performed as described previously.[66] Asynchronous blood stage *P. falciparum* cultures were plated at 1% parasitemia and 1% hematocrit in a 96-well plate and incubated with serial dilutions of compound for 72 h at 37 °C in 5% CO_2. DMSO concentrations were kept at a sublethal percentage (<0.2%). As a negative parasite growth control, 5 μM chloroquine was used. Plates were then frozen at −80 °C, thawed, and wells were given 100 μL of SYBR Green I-containing lysis buffer (20 mM Tris-HCl, 5 mM EDTA, 0.8% Triton X-100, 0.08% saponin, and 0.0001% SYBR Green I) (Thermo Fisher, Waltham, MA). After incubation for 45 min at room temperature protected from light, fluorescence emission was read with a multimode microplate reader (BioTek Synergy Neo2, Winooski, VT) at 485 nm excitation and 530 nm emission. The results were normalized using untreated and chloroquine-treated controls, and EC_{50} was determined with CDD Vault (www.collaborativedrug.com, Burlingame, CA).

Cytotoxicity Assay.

HepG2 cells were seeded at 2250 cells per well in a flat-bottomed black 384-well plate with a clear bottom and incubated at 37 °C with 5% CO_2. After 24 h, a serial dilution of compound was applied, and the plate was incubated further for 48 h. Negative control wells were treated with 5% Triton X-100 for 10 min, and 10 μL of MTS (3-(4,5-dimethylthiazol-2-yl)-5-(3-carboxymethoxyphenyl)-2-(4-sulfophenyl)-2*H*-tetrazolium) reagent (CellTiter 96 AQueous One Solution Reagent, Promega, Madison, WI) was added per well. After 3 h, the plate was read in a microplate reader (BioTek Synergy Neo2, Winooski, VT) at an absorbance of 490 nm. The results were normalized with untreated cells and Triton X-100-treated cells. EC_{50} was determined with a CDD Vault (Burlingame, CA).

Rate of Killing.

A flow-cytometry-based rate of killing assay was performed as described previously.[67] Asynchronous *P. falciparum* Dd2 cultures were plated at 1% parasitemia and 4% hematocrit into a 24-well plate. Wells were treated with $10 \times EC_{50}$ of compound for 12, 24, or 48 h before the compound was removed. Every 24 h thereafter for 4 days in total, culture samples were washed in 0.5% bovine serum albumin (BSA) and stained with $1\times$ SYBR Green I (Thermo Fisher, Waltham, MA) and 60 μM MitoTracker Deep Red FM (Thermo Fisher, Waltham, MA) for 20 min at 37 °C. After another wash in 0.5% BSA, samples were resuspended in phosphate-buffered saline (PBS) and analyzed via flow cytometry with a CytoFLEX S (Beckman Coulter, Brea, CA), with 100,000 events recorded per sample. For gating, the following controls were used: uninfected RBCs, untreated culture, DHA-treated culture, and untreated culture without MitoTracker stain. Viable parasite percentage was determined by finding the fraction of SYBR Green/MitoTracker double-positive cells from the total events. The analysis was performed with FlowJo software Version 10 (Ashland, OR).

Stage-Specific Assay.

The stage-specific assay was performed as previously described.[68] Asexual stage *P. falciparum* cultures were first synchronized by a MACS magnetic column (Miltenyi Biotec, Bergisch Gladbach, Germany), followed 3 h later by treatment with 5% sorbitol to select for rings.[69,70] Six hours after invasion, parasites were plated onto a 96-well plate at 1% parasitemia and 1% hematocrit, and the compound was added at $5 \times EC_{50}$ to the 6 HPI wells. Every 12 h, until reinvaded rings (54 HPI), thin blood smear slides for Giemsa stain were taken, and samples were washed and fixed in 4% paraformaldehyde in PBS with 0.04% glutaraldehyde. At the conclusion of the timepoints, all samples were permeabilized with 0.25% Triton X-100 before being treated with 50 μg/mL RNase A and stained with 500 nM YOYO-1 (Thermo Fisher, Waltham, MA). Samples were then washed, and flow cytometric analysis was performed with a CytoFLEX S (Beckman Coulter, Brea, CA), collecting 100,000 events per sample. The analysis was performed with FlowJo software Version 10.

Liver-Stage Activity Assay.

Assessment of activity in the liver stage was done as previously described. [71] Briefly, 3×10^3 of HepG2-A16-CD81 cells were seeded in 1536-well plates (Greiner Bio, Frickenhausen, Germany). Then, 50 nL of the test and control compounds were added in a 12-point 1:3 serial dilution. After 18 h, the cells are infected with 1×10^3 *P. berghei* sporozoites expressing luciferase. After 48 h post infection, 2 μL of luciferin reagent (BrightGlo, Promega, Madison, WI) was added to each well, and luciferase activity was detected using a PerkinElmer Envision plate reader. IC_{50} values were determined in CDD Vault (Burlingame, CA) normalized to maximum and minimum inhibition levels for the positive (Atovaquone 0.25 μM) and negative (DMSO) control wells.

ADP-Glo Kinase Assay.

Activities of compounds **1**, **11**, and **12** were evaluated in recombinant *Pf*ARK2-GST and human AurA-GST, which is a kind gift from the laboratory of Dr. Ratna Chakrabarti. Assays were performed in 384-well white round-bottom plates, with a final reaction volume of 10 μL. For both kinases, reactions were comprised of 1× Kinase Buffer (Cell Signaling) and 10 μM ATP (Thermo Fisher, Waltham, MA), with 2 μg of the substrate and 0.4 μg of kinase. For *Pf*ARK2, the substrate is dephosphorylated MBP (#31314, ActiveMotif, Carlsbad, CA), and for human AurA, the substrate is cofilin (a gift from the Dr. R. Chakrabarti Laboratory). Inhibitors were added as a serial dilution of 1:3 beginning with 5 μM final concentration, followed by the buffer and enzyme. After 10 min of room-temperature incubation, the ATP and substrate were added, and the reactions were left to incubate for 45 min at 25 °C. Next, 10 μL of ADP-Glo Reagent per well was added to stop the reaction, and the plate was incubated at room temperature for 40 min. Next, 20 μL of Kinase Detection Reagent per well was added, and luminescence was evaluated with a multimode microplate reader (BioTek Synergy Neo2, Winooski, VT). All reactions were performed in duplicate. Per kinase, reactions without inhibitor served as a 100% activity control, and reactions without kinase served as 0% activity controls. The known human AurA inhibitor,

VX680 (#HY-10161, MedChemExpress, Monmouth Junction, NJ), was a control for AurA inhibition. Analysis and graphing were generated with GraphPad Prism 9 (San Diego, CA).

Resistance Line Generation and Genomic Analysis.

Resistant parasites were selected with three parental clones: 3D7 clone A10, Dd2 clone B2, and Dd2-pol delta clone H11. For each selection, three independent flasks containing 107 parasites were exposed to BI-2536 for 3–5 days at EC_{50} concentrations for each parasite clone (288 nM for 3D7, 371 nM for Dd2, and 256 nM for Dd2-pol delta). BI-2536 was removed from the culture media once parasite replication stopped and was started again after parasites resumed to replicate well. The drug off–drug on cycles were continued for 8 months of culturing. During this time, the concentration of BI-2536 was gradually increased (in ~10% steps) until a concentration of 1.8 μM. For each of the different three parental parasite lines, all three flasks yielded compound-resistant parasites. Two flasks originating from 3D7-A10 and three flasks originating from Dd2-B2 were subjected to WGS, while clonal parasites were obtaining from two independent selections with Dd2-pol delta parasites. For Dd2-pol delta parasites, two clones each from two independent selections were sequenced. Genomic DNA (gDNA) was obtained from parasite samples by washing infected RBCs with 0.05% saponin and isolating using the DNeasy Blood and Tissue Kit (Qiagen) following standard protocols. Sequencing libraries were prepared by the UCSD Institute for Genomic Medicine (IGM) Genomics Center using the Nextera XT kit (#FC-131–1024, Illumina, San Diego, CA) and were sequenced on lllumina NovaSeq. 6000 (S4 200, PE100). Sequencing reads were aligned to the *P. falciparum* 3D7 reference genome (PlasmoDB v13.0) and preprocessed following standard GATK version 3.5 protocols.[72,73] SNVs and INDELs were called with GATK HaplotypeCaller and filtered to retain high-quality variants as previously described.[74] CNVs were detected by the GATK 4 workflow[72] adapted for *P. falciparum* as described in Summers et al.[75] Briefly, read counts were collected across the genic regions of the *P. falciparum* core genome[76] and denoised log 2 copy ratios were calculated against a panel of normals constructed from nondrug-selected 3D7 and Dd2 samples. CNVs were retained if at least four sequential genes showed a denoised log 2 copy ratio greater than or equal to 0.5 (copy number increase).

Western Blot Analysis of eIF2α Phosphorylation.

Flasks of *P. falciparum* Dd2 cultures at 4% hematocrit were sorbitol-synchronized as described above, and cultures were predominantly ring to early trophozoite stages and ~10% parasitemia were treated for 3 h with compound **1** at three concentrations: 10, 1, and 0.1 μM. Borrelidin (SC-200379, Santa Cruz Biotechnology, Dallas, TX) and halofuginone (#55837–20-2, MedChemExpress, Monmouth Junction, NJ) at 200 nM each served as positive controls for eIF2α phosphorylation, and DMSO at 0.1% served as a vehicle control. After incubation, RBCs were lysed with 0.1% saponin and washed three times with Dulbecco's phosphate buffer (DPBS). Pellets were frozen at −80 °C, thawed on ice, and resuspended in Pierce RIPA buffer (#89900, Thermo Fisher, Waltham, MA) supplemented with 1× Halt Protease & Phosphatase Inhibitor Cocktail (#78443, Thermo Fisher, Waltham, MA). Pellets were incubated on ice for 30 min with periodic vortexing, and lysate cleared with centrifugation at 4 °C at 15 000g for 10 min. After quantification with the Pierce BCA Protein Assay (#23227, Thermo Fisher, Waltham, MA), 30 μg protein per sample was

given 1× NuPAGE loading dye (Invitrogen, Waltham, MA) and boiled for 7 min at 80°
and loaded onto a 12% Bis–Tris sodium dodecyl sulfate polyacrylamide gel electrophoresis
(SDS-PAGE) gel. After electrophoresis, the proteins were blotted onto a poly-(vinylidene
fluoride) (PVDF) membrane via the BioRad TransBlot Turbo system and blocked at room
temperature for 1 h with 5% milk in tris-buffered saline with 0.1% Tween 20 (TBST).
Primary antibody incubations were performed overnight at 4 °C, and secondary antibody
incubations were performed at room temperature for 1 h. Between incubations, membranes
were washed with TBST 3 × 5 min at room temperature. Rabbit antiphospho-eIF2 (Ser51)
primary antibodies (#3597, Cell Signaling) were diluted 1:1000 in 5% BSA in TBST,
and anti-rabbit HRP-conjugated secondary antibodies (#7074, Cell Signaling) were diluted
1:20,000 in 5% milk in TBST. Rat anti-BiP primary antibodies (BEI, MRA-1247) were
diluted 1:10,000 in 5% milk in TBST and anti-rat HRP-conjugated secondary antibodies
(#AP136P, MilliporeSigma, Burlington, MA). Development was performed using the
SuperSignal West PLUS Chemiluminescent Substrate (Thermo Fisher, Waltham, MA) and
the ChemiDoc MP imaging system (BioRad, Hercules, CA).

Split-Luciferase Assay.

This assay was performed by Luceome Biotechnologies (Tuscon, AZ) as fee per service,
using a method previously described.[17] The KinaseSeeker Assay offers a panel of 11 *P.
falciparum* kinases, and initially, the compounds are scanned at a fixed concentration of
2.5 μM, and subsequently, an IC_{50} determination can be made using an eight-point dilution
series.

Recombinant Protein Production.

The full coding sequencing (CDS) of *Pf*NEK3, aside from the first 10 residues on the
N-terminus, cloned in a pGEX-4T-3 vector, was a generous gift from Christian Doerig.
The *Pf*ARK2-GST construct was generated within the Chakrabarti laboratory, and cloning
is described in the Supporting Information. *E. coli* BL21(DE3) competent cells (Agilent,
Santa Clara, CA) were transformed via heat shock, and expression was induced with 1 mM
IPTG at 20 °C for 16 h. Bacterial lysates were pelleted by centrifugation and resuspended
in a HEPES salt buffer (50 mM HEPES, 200 mM NaCl, 0.02% monothiolglycerol, pH 7.5)
supplemented with 1× HALT Protease Inhibitor (#78443, Thermo Fisher, Waltham, MA).
Lysis was achieved with French press and sonication, and the lysate was clarified with
centrifugation and filtration through a 0.2 μm PES membrane. Total protein lysate was run
through a GSTrap FF Column (Cytiva, Marlborough, MA) and eluted with the suspension
buffer supplemented with 20 mM glutathione. The resulting fractions were desalted with
PD-10 Columns (Cytiva, Marlborough, MA) and quantified with a Bradford protein assay in
accordance with the manufacturer's protocol (BioRad, Hercules, CA).

Radioactive Kinase Assays.

For *Pf*NEK3, individual reactions were prepared in 15 μL, for a final concentration of
1× Kinase Buffer (Cell Signaling), 10 mM MnCl 2, 5 μg of dephosphorylated MBP
(#31314, ActiveMotif, Carlsbad, CA), 1.5 μg of purified recombinant *Pf*NEK3-GST, 10
μM ATP (Thermo Fisher, Waltham, MA), and 0.1 μM γ–^{32}P ATP (3000Ci/mmol 10mCi/ml
EasyTide, PerkinElmer, Waltham, MA). For *Pf*ARK2, reactions were prepared in 20 μL

with 1×Kinase Buffer, 0.5 μg of purified recombinant *Pf*ARK2-GST, 5 μg of MBP, 10 μM ATP, and 0.1 μM γ-^{32} P ATP. Reaction tubes were incubated for 30 min at 30 °C in a water bath before adding 4 μL of 4× NuPAGE loading dye (Invitrogen, Waltham, MA) and boiling for 7 min at 80 °C. The samples were cooled and run on a 12% Bis–Tris SDS-PAGE gel impregnated with 2,2,2-trichloroethanol (TCE). Protein concentration was determined by UV imaging on a ChemiDoc XRS+ Imaging System (BioRad, Hercules, CA). Proteins were blotted onto a PVDF membrane with the BioRad TransBlot Turbo system. Membranes were dried and incubated overnight with a phosphoscreen before imaging with a Personal Molecular Imager (BioRad, Hercules, CA). Densiometric analysis of the TCE gel and membrane was performed with Image Lab 6.1 software (BioRad, Hercules, CA), and correlation plots were generated with GraphPad Prism 9 (San Diego, CA).

Phosphoproteomics Sample Preparation.

Three flasks of asynchronous blood stage *P. falciparum* Dd2 culture were grown to ~15% parasitemia and 4% hematocrit under standard culture conditions. Per biological replicate, media was aspirated and replaced with fresh culture media, supplemented with either 5 × EC_{50} or EC_{90} depending on the slope of the EC_{50} curve. As a control, culture was treated with an equal volume of DMSO vehicle (0.04% final concentration). After 3 h, parasites were collected as described above through saponin lysis of erythrocytes. Parasite pellets were resuspended in freshly made 8 M urea lysis buffer (8 M urea, 50 mM Tris pH 8. 5, 1% SDS) supplemented with 1× HALT Protease & Phosphatase Inhibitor Cocktail (#78443, Thermo Fisher, Waltham, MA). The parasites were lysed by sonication, and the protein was quantified with the Pierce BCA Protein Assay (#23227, Thermo Fisher, Waltham, MA). The lysate was stored at −80 °C until processing at the Thermo Fisher Center for Multiplexed Proteomics (TCMP) at HMS. At this time, the samples were reduced, alkylated, resuspended, and digested.[77] The resulting peptides were quantified and labeled with isobaric tandem mass tags (TMT).[46] Following a ratio check, phosphoenrichment was performed with a Pierce High-Select Fe-NTA Phosphopeptide Enrichment Kit (Thermo Fisher, Waltham, MA). The resultant phosphopeptide eluate was analyzed with LC-MS2. The peptide flowthrough was fractionated by basic reverse-phase HPLC and similarly analyzed with LC-MS3. Spectra were searched against a composite *P. falciparum* and human Uniprot database (https://www.uniprot.org/) using the COMET algorithm.[78] Peptide matches were filtered with a 1% false discovery rate (FDR), and peptides with a summed signal-to-noise (SN) threshold of >100 were quantified. For phosphopeptides, a 1% FDR filter and a summed SN threshold of   100 were used. Data will be released in the MassIVE repository upon publication.

Phosphoproteomics Analysis.

The analysis was performed with normalized relative abundance values obtained from the TCMP. Only results with more than one peptide were considered, and *Z*-score from ratio-based paired *Z*-test ($Z = (\log 2(r) - 0)/(\delta/\ n)$), where *r* is the mean of treated/untreated ratios. GraphPad Prism 9 was used to generate the volcano plots (San Diego, CA). Disruptability of proteins was determined through the PhenoPlasm database (http://phenoplasm.org).[79] GO-term analysis was performed using gene identifiers of the proteins containing at least one of the 10% most differential phosphorylation sites ($|\log 2(fc)| > 0.585$). Significantly

enriched GO terms were obtained using the PlasmoDB Gene Ontology Enrichment tool, which uses the background data set with the *P. falciparum* 3D7 genome and the Fisher's Exact test to identify these terms (http://PlasmoDB.org).[80] REVIGO[81] was then used to remove obsolete or redundant terms and cluster similar terms, and the remaining terms were graphed with Cytoscape version 3.9.[82] STRING analysis was performed on all top-ranked differentially expressed phosphosites (highest 10% $|Z$-score$|$ and $|\log 2(fc)| > 0.585$) with the addition of *Pf*NEK3 (https://string-db.org/).[83] Interactomes for each treatment individually and the shared interactome were considered. The results were transferred into Cytoscape version 3.9,[82] and all edges with a minimum interaction of 0.2 were including in groupings. Edge color represented the greatest contribution source for STRING score, and the overall score was indicated by edge thickness. PPI enrichment score was determined based on a more stringent interaction score of 0.4. Legend was created in BioRender (Biorender.com).

Supplementary Material

Refer to Web version on PubMed Central for supplementary material.

ACKNOWLEDGMENTS

ABBREVIATIONS

P. falciparum	*Plasmodium falciparum*
PLK	Polo-like kinase
NEK	NIMA-related kinase
EC$_{50}$	half-maximal effective concentration
IC$_{50}$	half-maximal inhibitory concentration
RI	resistance index
SI	selectivity index
HPI	hours post invasion
ARKs	Aurora-related kinases

MAPK	mitogen-activated protein kinase
MPB	myelin basic protein
SNP	single nucleotide polymorphism
WGS	whole genome sequencing
aaRS	aminoacyl-tRNA synthetase
PDB	Research Collaboratory for Structural Bioinformatics Protein Data Bank
HPLC	high-pressure liquid chromatography
IMAC	immobilized metal affinity chromatography
GO	gene ontology
BCA assay	bicinchoninic acid assay
TBST	tris-buffered saline with 0.1% Tween 20
BSA	bovine serum albumin

REFERENCES

(1). Organization, W. H. World Health Organization (WHO). World Malaria Report 2021, 2021.

(2). Dondorp AM; Nosten F; Yi P; Das D; Phyo AP; Tarning J; Lwin KM; Ariey F; Hanpithakpong W; Lee SJ; Ringwald P; Silamut K; Imwong M; Chotivanich K; Lim P; Herdman T; An SS; Yeung S; Singhasivanon P; Day NP; Lindegardh N; Socheat D; White NJ Artemisinin resistance in *Plasmodium falciparum* malaria. N. Engl. J. Med 2009, 361, 455–467. [PubMed: 19641202]

(3). Uwimana A; Legrand E; Stokes BH; Ndikumana JM; Warsame M; Umulisa N; Ngamije D; Munyaneza T; Mazarati JB; Munguti K; Campagne P; Criscuolo A; Ariey F; Murindahabi M; Ringwald P; Fidock DA; Mbituyumuremyi A; Menard D Emergence and clonal expansion of in vitro artemisinin-resistant *Plasmodium falciparum* kelch13 R561H mutant parasites in Rwanda. Nat. Med 2020, 26, 1602–1608. [PubMed: 32747827]

(4). Arendse LB; Wyllie S; Chibale K; Gilbert IH Plasmodium Kinases as Potential Drug Targets for Malaria: Challenges and Opportunities. ACS Infect. Dis 2021, 7, 518–534. [PubMed: 33590753]

(5). Cohen P; Cross D; Janne PA Kinase drug discovery 20 years after imatinib: progress and future directions. Nat. Rev. Drug Discovery 2021, 20, 551–569. [PubMed: 34002056]

(6). Derbyshire ER; Zuzarte-Luis V; Magalhaes AD; Kato N; Sanschagrin PC; Wang J; Zhou W; Miduturu CV; Mazitschek R; Sliz P; Mota MM; Gray NS; Clardy J Chemical interrogation of the malaria kinome. ChemBioChem 2014, 15, 1920–1930. [PubMed: 25111632]

(7). Steegmaier M; Hoffmann M; Baum A; Lenart P; Petronczki M; Krssak M; Gurtler U; Garin-Chesa P; Lieb S; Quant J; Grauert M; Adolf GR; Kraut N; Peters JM; Rettig WJ BI 2536, a potent and selective inhibitor of polo-like kinase 1, inhibits tumor growth in vivo. Curr. Biol 2007, 17, 316–322. [PubMed: 17291758]

(8). Miranda-Saavedra D; Gabaldon T; Barton GJ; Langsley G; Doerig C The kinomes of apicomplexan parasites. Microbes Infect. 2012, 14, 796–810. [PubMed: 22587893]

(9). Barr FA; Sillje HH; Nigg EA Polo-like kinases and the orchestration of cell division. Nat. Rev. Mol. Cell Biol 2004, 5, 429–440. [PubMed: 15173822]

(10). Hanson KK; Ressurreicao AS; Buchholz K; Prudencio M; Herman-Ornelas JD; Rebelo M; Beatty WL; Wirth DF; Hanscheid T; Moreira R; Marti M; Mota MM Torins are potent antimalarials that block replenishment of Plasmodium liver stage parasitophorous vacuole

membrane proteins. Proc. Natl. Acad. Sci. U.S.A 2013, 110, E2838–E2847. [PubMed: 23836641]

(11). Murillo-Solano C; Dong C; Sanchez CG; Pizarro JC Identification and characterization of the antiplasmodial activity of Hsp90 inhibitors. Malar. J 2017, 16, No. 292. [PubMed: 28724415]

(12). Adderley JD; John von Freyend S; Jackson SA; Bird MJ; Burns AL; Anar B; Metcalf T; Semblat JP; Billker O; Wilson DW; Doerig C Analysis of erythrocyte signalling pathways during *Plasmodium falciparum* infection identifies targets for host-directed antimalarial intervention. Nat. Commun 2020, 11, No. 4015. [PubMed: 32782246]

(13). Vaid A; Thomas DC; Sharma P Role of Ca2+/calmodulin-PfPKB signaling pathway in erythrocyte invasion by *Plasmodium falciparum*. J. Biol. Chem 2008, 283, 5589–5597. [PubMed: 18165240]

(14). Mott BT; Eastman RT; Guha R; Sherlach KS; Siriwardana A; Shinn P; McKnight C; Michael S; Lacerda-Queiroz N; Patel PR; Khine P; Sun H; Kasbekar M; Aghdam N; Fontaine SD; Liu D; Mierzwa T; Mathews-Griner LA; Ferrer M; Renslo AR; Inglese J; Yuan J; Roepe PD; Su XZ; Thomas CJ High-throughput matrix screening identifies synergistic and antagonistic antimalarial drug combinations. Sci. Rep 2015, 5, No. 13891. [PubMed: 26403635]

(15). Miduturu CV; Deng X; Kwiatkowski N; Yang W; Brault L; Filippakopoulos P; Chung E; Yang Q; Schwaller J; Knapp S; King RW; Lee JD; Herrgard S; Zarrinkar P; Gray NS High-throughput kinase profiling: a more efficient approach toward the discovery of new kinase inhibitors. Chem. Biol 2011, 18, 868–879. [PubMed: 21802008]

(16). Deng Z; Chen G; Liu S; Li Y; Zhong J; Zhang B; Li L; Huang H; Wang Z; Xu Q; Deng X Discovery of methyl 3-((2-((1-(dimethylglycyl)-5-methoxyindolin-6-yl)amino)-5-(trifluoromethyl) pyrimidin-4-yl)amino)thiophene-2-carboxylate as a potent and selective polo-like kinase 1 (PLK1) inhibitor for combating hepatocellular carcinoma. Eur. J. Med. Chem 2020, 206, No. 112697. [PubMed: 32814244]

(17). Jester BW; Cox KJ; Gaj A; Shomin CD; Porter JR; Ghosh I A coiled-coil enabled split-luciferase three-hybrid system: applied toward profiling inhibitors of protein kinases. J. Am. Chem. Soc 2010, 132, 11727–11735. [PubMed: 20669947]

(18). Davis MI; Hunt JP; Herrgard S; Ciceri P; Wodicka LM; Pallares G; Hocker M; Treiber DK; Zarrinkar PP Comprehensive analysis of kinase inhibitor selectivity. Nat. Biotechnol 2011, 29, 1046–1051. [PubMed: 22037378]

(19). Dorin-Semblat D; Schmitt S; Semblat JP; Sicard A; Reininger L; Goldring D; Patterson S; Quashie N; Chakrabarti D; Meijer L; Doerig C *Plasmodium falciparum* NIMA-related kinase Pfnek-1: sex specificity and assessment of essentiality for the erythrocytic asexual cycle. Microbiology 2011, 157, 2785–2794. [PubMed: 21757488]

(20). Reininger L; Tewari R; Fennell C; Holland Z; Goldring D; Ranford-Cartwright L; Billker O; Doerig C An essential role for the Plasmodium Nek-2 Nima-related protein kinase in the sexual development of malaria parasites. J. Biol. Chem 2009, 284, 20858–20868. [PubMed: 19491095]

(21). Reininger L; Garcia M; Tomlins A; Muller S; Doerig C The *Plasmodium falciparum*, Nima-related kinase Pfnek-4: a marker for asexual parasites committed to sexual differentiation. Malar. J 2012, 11, No. 250. [PubMed: 22849771]

(22). Lye YM; Chan M; Sim TS Pfnek3: an atypical activator of a MAP kinase in *Plasmodium falciparum*. FEBS Lett. 2006, 580, 6083–6092. [PubMed: 17064692]

(23). Solyakov L; Halbert J; Alam MM; Semblat JP; Dorin-Semblat D; Reininger L; Bottrill AR; Mistry S; Abdi A; Fennell C; Holland Z; Demarta C; Bouza Y; Sicard A; Nivez MP; Eschenlauer S; Lama T; Thomas DC; Sharma P; Agarwal S; Kern S; Pradel G; Graciotti M; Tobin AB; Doerig C Global kinomic and phospho-proteomic analyses of the human malaria parasite *Plasmodium falciparum*. Nat. Commun 2011, 2, No. 565. [PubMed: 22127061]

(24). Zhang M; Wang C; Otto TD; Oberstaller J; Liao X; Adapa SR; Udenze K; Bronner IF; Casandra D; Mayho M; Brown J; Li S; Swanson J; Rayner JC; Jiang RHY; Adams JH Uncovering the essential genes of the human malaria parasite *Plasmodium falciparum* by saturation mutagenesis. Science 2018, 360, No. eaap7847. [PubMed: 29724925]

(25). Low H; Chua CS; Sim TS *Plasmodium falciparum* possesses a unique dual-specificity serine/threonine and tyrosine kinase, Pfnek3. Cell. Mol. Life Sci 2012, 69, 1523–1535. [PubMed: 22116321]

(26). Ward P; Equinet L; Packer J; Doerig C Protein kinases of the human malaria parasite *Plasmodium falciparum*: the kinome of a divergent eukaryote. BMC Genomics 2004, 5, No. 79. [PubMed: 15479470]

(27). Hitz E; Balestra AC; Brochet M; Voss TS PfMAP-2 is essential for male gametogenesis in the malaria parasite *Plasmodium falciparum*. Sci. Rep 2020, 10, No. 11930. [PubMed: 32681115]

(28). Morahan BJ; Abrie C; Al-Hasani K; Batty MB; Corey V; Cowell AN; Niemand J; Winzeler EA; Birkholtz LM; Doerig C; Garcia-Bustos JF Human Aurora kinase inhibitor Hesperadin reveals epistatic interaction between *Plasmodium falciparum* PfArk1 and PfNek1 kinases. Commun. Biol 2020, 3, No. 701. [PubMed: 33219324]

(29). Reininger L; Wilkes JM; Bourgade H; Miranda-Saavedra D; Doerig C An essential Aurora-related kinase transiently associates with spindle pole bodies during *Plasmodium falciparum* erythrocytic schizogony. Mol. Microbiol 2011, 79, 205–221. [PubMed: 21166904]

(30). Ember SWJ; Zhu JY; Olesen SH; Martin MP; Becker A; Berndt N; Georg GI; Schonbrunn E Acetyl-lysine binding site of bromodomain-containing protein 4 (BRD4) interacts with diverse kinase inhibitors. ACS Chem. Biol 2014, 9, 1160–1171. [PubMed: 24568369]

(31). Ciceri P; Muller S; O'Mahony A; Fedorov O; Filippakopoulos P; Hunt JP; Lasater EA; Pallares G; Picaud S; Wells C; Martin S; Wodicka LM; Shah NP; Treiber DK; Knapp S Dual kinase-bromodomain inhibitors for rationally designed polypharmacology. Nat. Chem. Biol 2014, 10, 305–312. [PubMed: 24584101]

(32). Munoz L Non-kinase targets of protein kinase inhibitors. Nat. Rev. Drug Discovery 2017, 16, 424–440. [PubMed: 28280261]

(33). Hui DF; Fonesca M; Josling G; Tallant C; Wernimont A; Fedorov O; Hutchinson A; Loppnau P; Duffy M; Knapp S; Raymond H Plasmodium bromodomain PfBDP4; A Target Enabling Package (Version 5) [Data set]. Zenodo 2016, DOI: 10.5281/zenodo.1209237.

(34). Chua MJ; Robaa D; Skinner-Adams TS; Sippl W; Andrews KT Activity of bromodomain protein inhibitors/binders against asexual-stage *Plasmodium falciparum* parasites. Int. J. Parasitol.: Drugs Drug Resist 2018, 8, 189–193. [PubMed: 29631126]

(35). Nguyen HHT; Yeoh LM; Chisholm SA; Duffy MF Developments in drug design strategies for bromodomain protein inhibitors to target Plasmodium falciparum parasites. Expert Opin. Drug Discovery 2020, 15, 415–425.

(36). Qiu D; Pei JV; Rosling JEO; Li D; Xue Y; Penington JS; Kümpornsin K; Vincent Aw YT; Han Aw JY; Hasemer H; Dennis ASM; Ridgway MC; Papenfuss AT; Lee MCS; van Dooren GG; Kirk K; Lehane AM Generation and character-isation of *P. falciparum* parasites with a G358S mutation in the PfATP4 Na+ pump and clinically relevant levels of resistance to some PfATP4 inhibitors. bioRxiv 2022, 2022.2001.2011.475938.

(37). Koenderink JB; Kavishe RA; Rijpma SR; Russel FG The ABCs of multidrug resistance in malaria. Trends Parasitol. 2010, 26, 440–446. [PubMed: 20541973]

(38). Murithi JM; Deni I; Pasaje CFA; Okombo J; Bridgford JL; Gnadig NF; Edwards RL; Yeo T; Mok S; Burkhard AY; Coburn-Flynn O; Istvan ES; Sakata-Kato T; Gomez-Lorenzo MG; Cowell AN; Wicht KJ; Le Manach C; Kalantarov GF; Dey S; Duffey M; Laleu B; Lukens AK; Ottilie S; Vanaerschot M; Trakht IN; Gamo FJ; Wirth DF; Goldberg DE; Odom John AR; Chibale K; Winzeler EA; Niles JC; Fidock DA The *Plasmodium falciparum* ABC transporter ABCI3 confers parasite strain-dependent pleiotropic antimalarial drug resistance. Cell Chem. Biol 2022, 29, 824–839.e6. [PubMed: 34233174]

(39). Navale R; Atul; Allanki AD; Sijwali PS Characterization of the autophagy marker protein Atg8 reveals atypical features of autophagy in *Plasmodium falciparum*. PLoS One 2014, 9, No. e113220. [PubMed: 25426852]

(40). Holcik M; Sonenberg N Translational control in stress and apoptosis. Nat. Rev. Mol. Cell Biol 2005, 6, 318–327. [PubMed: 15803138]

(41). Fennell C; Babbitt S; Russo I; Wilkes J; Ranford-Cartwright L; Goldberg DE; Doerig C PfeIK1, a eukaryotic initiation factor 2alpha kinase of the human malaria parasite *Plasmodium falciparum*, regulates stress-response to amino-acid starvation. Malar. J 2009, 8, 99. [PubMed: 19435497]

(42). Zhang M; Fennell C; Ranford-Cartwright L; Sakthivel R; Gueirard P; Meister S; Caspi A; Doerig C; Nussenzweig RS; Tuteja R; Sullivan WJ Jr.; Roos DS; Fontoura BM; Menard R; Winzeler EA; Nussenzweig V The Plasmodium eukaryotic initiation factor-2a kinase IK2 controls the latency of sporozoites in the mosquito salivary glands. J. Exp. Med 2010, 207, 1465–1474. [PubMed: 20584882]

(43). Zhang M; Mishra S; Sakthivel R; Rojas M; Ranjan R; Sullivan WJ Jr.; Fontoura BM; Menard R; Dever TE; Nussenzweig V PK4, a eukaryotic initiation factor 2alpha(eIF2alpha) kinase, is essential for the development of the erythrocytic cycle of Plasmodium. Proc. Natl. Acad. Sci. U.S.A 2012, 109, 3956–3961. [PubMed: 22355110]

(44). Ishiyama A; Iwatsuki M; Namatame M; Nishihara-Tsukashima A; Sunazuka T; Takahashi Y; Omura S; Otoguro K Borrelidin, a potent antimalarial: stage-specific inhibition profile of synchronized cultures of *Plasmodium falciparum*. J. Antibiot 2011, 64, 381–384.

(45). Keller TL; Zocco D; Sundrud MS; Hendrick M; Edenius M; Yum J; Kim YJ; Lee HK; Cortese JF; Wirth DF; Dignam JD; Rao A; Yeo CY; Mazitschek R; Whitman M Halofuginone and other febrifugine derivatives inhibit prolyl-tRNA synthetase. Nat. Chem. Biol 2012, 8, 311–317. [PubMed: 22327401]

(46). Li J; Van Vranken JG; Pontano Vaites L; Schweppe DK; Huttlin EL; Etienne C; Nandhikonda P; Viner R; Robitaille AM; Thompson AH; Kuhn K; Pike I; Bomgarden RD; Rogers JC; Gygi SP; Paulo JA TMTpro reagents: a set of isobaric labeling mass tags enables simultaneous proteome-wide measurements across 16 samples. Nat. Methods 2020, 17, 399–404. [PubMed: 32203386]

(47). Szklarczyk D; Gable AL; Lyon D; Junge A; Wyder S; Huerta-Cepas J; Simonovic M; Doncheva NT; Morris JH; Bork P; Jensen LJ; Mering CV STRING v11: protein-protein association networks with increased coverage, supporting functional discovery in genome-wide experimental datasets. Nucleic Acids Res. 2019, 47, D607–D613. [PubMed: 30476243]

(48). Paul AS; Miliu A; Paulo JA; Goldberg JM; Bonilla AM; Berry L; Seveno M; Braun-Breton C; Kosber AL; Elsworth B; Arriola JSN; Lebrun M; Gygi SP; Lamarque MH; Duraisingh MT Co-option of *Plasmodium falciparum* PP1 for egress from host erythrocytes. Nat. Commun 2020, 11, No. 3532. [PubMed: 32669539]

(49). Rudlaff RM; Kraemer S; Streva VA; Dvorin JD An essential contractile ring protein controls cell division in *Plasmodium falciparum*. Nat. Commun 2019, 10, No. 2181. [PubMed: 31097714]

(50). Birnbaum J; Scharf S; Schmidt S; Jonscher E; Hoeijmakers WAM; Flemming S; Toenhake CG; Schmitt M; Sabitzki R; Bergmann B; Frohlke U; Mesen-Ramirez P; Blancke Soares A; Herrmann H; Bartfai R; Spielmann T A Kelch13-defined endocytosis pathway mediates artemisinin resistance in malaria parasites. Science 2020, 367, 51–59. [PubMed: 31896710]

(51). Bennink S; Pradel G The molecular machinery of translational control in malaria parasites. Mol. Microbiol 2019, 112, 1658–1673. [PubMed: 31531994]

(52). Hart KJ; Power BJ; Rios KT; Sebastian A; Lindner SE The Plasmodium NOT1-G paralogue is an essential regulator of sexual stage maturation and parasite transmission. PLoS Biol. 2021, 19, No. e3001434. [PubMed: 34673764]

(53). Baumgarten S; Bryant JM; Sinha A; Reyser T; Preiser PR; Dedon PC; Scherf A Transcriptome-wide dynamics of extensive m(6)A mRNA methylation during *Plasmodium falciparum* blood-stage development. Nat. Microbiol 2019, 4, 2246–2259. [PubMed: 31384004]

(54). The Plasmodium Genome Database Collaborative. PlasmoDB: An integrative database of the *Plasmodium falciparum* genome. Tools for accessing and analyzing finished and unfinished sequence data. Nucleic Acids Res. 2001, 29, 66–69. [PubMed: 11125051]

(55). Tewari R; Straschil U; Bateman A; Bohme U; Cherevach I; Gong P; Pain A; Billker O The systematic functional analysis of Plasmodium protein kinases identifies essential regulators of mosquito transmission. Cell Host Microbe 2010, 8, 377–387. [PubMed: 20951971]

(56). Wang G; Jiang Q; Zhang C The role of mitotic kinases in coupling the centrosome cycle with the assembly of the mitotic spindle. J. Cell Sci 2014, 127, 4111–4122. [PubMed: 25128564]

(57). Zitouni S; Nabais C; Jana SC; Guerrero A; Bettencourt-Dias M Polo-like kinases: structural variations lead to multiple functions. Nat. Rev. Mol. Cell Biol 2014, 15, 433–452. [PubMed: 24954208]

(58). Matthews H; Duffy CW; Merrick CJ Checks and balances? DNA replication and the cell cycle in Plasmodium. Parasites Vectors 2018, 11, No. 216. [PubMed: 29587837]

(59). Carvalho TG; Doerig C; Reininger L Nima- and Aurora-related kinases of malaria parasites. Biochim. Biophys. Acta, Proteins Proteomics 2013, 1834, 1336–1345.

(60). Francia ME; Striepen B Cell division in apicomplexan parasites. Nat. Rev. Microbiol 2014, 12, 125–136. [PubMed: 24384598]

(61). Anighoro A; Bajorath J; Rastelli G Polypharmacology: challenges and opportunities in drug discovery. J. Med. Chem 2014, 57, 7874–7887. [PubMed: 24946140]

(62). Khan S Recent advances in the biology and drug targeting of malaria parasite aminoacyl-tRNA synthetases. Malar. J 2016, 15, No. 203. [PubMed: 27068331]

(63). Xie SC; Metcalfe RD; Dunn E; Morton CJ; Huang SC; Puhalovich T; Du Y; Wittlin S; Nie S; Luth MR; Ma L; Kim MS; Pasaje CFA; Kumpornsin K; Giannangelo C; Houghton FJ; Churchyard A; Famodimu MT; Barry DC; Gillett DL; Dey S; Kosaisih CC; Newman W; Niles JC; Lee MCS; Baum J; Ottilie S; Winzeler EA; Creek DJ; Williamson N; Parker MW; Brand S; Langston SP; Dick LR; Griffin MDW; Gould AE; Tilley L Reaction hijacking of tyrosine tRNA synthetase as a new whole-of-life-cycle antimalarial strategy. Science 2022, 376, 1074–1079. [PubMed: 35653481]

(64). Zhou J; Huang Z; Zheng L; Hei Z; Wang Z; Yu B; Jiang L; Wang J; Fang P Inhibition of *Plasmodium falciparum* Lysyl-tRNA synthetase via an anaplastic lymphoma kinase inhibitor. Nucleic Acids Res. 2020, 48, 11566–11576. [PubMed: 33053158]

(65). Trager W; Jensen JB Human malaria parasites in continuous culture. Science 1976, 193, 673–675. [PubMed: 781840]

(66). Dery V; Duah NO; Ayanful-Torgby R; Matrevi SA; Anto F; Quashie NB An improved SYBR Green-1-based fluorescence method for the routine monitoring of *Plasmodium falciparum* resistance to anti-malarial drugs. Malar. J 2015, 14, No. 481. [PubMed: 26625907]

(67). Clements RL; Streva V; Dumoulin P; Huang W; Owens E; Raj DK; Burleigh B; Llinas M; Winzeler EA; Zhang Q; Dvorin JD A Novel Antiparasitic Compound Kills Ring-Stage *Plasmodium falciparum* and Retains Activity Against Artemisinin-Resistant Parasites. J. Infect. Dis 2020, 221, 956–962. [PubMed: 31616928]

(68). Wright AE; Collins JE; Roberts B; Roberts JC; Winder PL; Reed JK; Diaz MC; Pomponi SA; Chakrabarti D Antiplasmodial Compounds from Deep-Water Marine Invertebrates. Mar. Drugs 2021, 19, 179. [PubMed: 33805935]

(69). Mata-Cantero L; Lafuente MJ; Sanz L; Rodriguez MS Magnetic isolation of *Plasmodium falciparum* schizonts iRBCs to generate a high parasitaemia and synchronized in vitro culture. Malar.J 2014, 13, No. 112. [PubMed: 24655321]

(70). Lambros C; Vanderberg JP Synchronization of *Plasmodium falciparum* erythrocytic stages in culture. J Parasitol. 1979, 65, 418–420. [PubMed: 383936]

(71). Antonova-Koch Y; Meister S; Abraham M; Luth MR; Ottilie S; Lukens AK; Sakata-Kato T; Vanaerschot M; Owen E; Jado JC; Maher SP; Calla J; Plouffe D; Zhong Y; Chen K; Chaumeau V; Conway AJ; McNamara CW; Ibanez M; Gagaring K; Serrano FN; Eribez K; Taggard CM; Cheung AL; Lincoln C; Ambachew B; Rouillier M; Siegel D; Nosten F; Kyle DE; Gamo FJ; Zhou Y; Llinas M; Fidock DA; Wirth DF; Burrows J; Campo B; Winzeler EA Open-source discovery of chemical leads for next-generation chemoprotective antimalarials. Science 2018, 362, No. eaat9446. [PubMed: 30523084]

(72). McKenna A; Hanna M; Banks E; Sivachenko A; Cibulskis K; Kernytsky A; Garimella K; Altshuler D; Gabriel S; Daly M; DePristo MA The Genome Analysis Toolkit: a MapReduce framework for analyzing next-generation DNA sequencing data. Genome Res. 2010, 20, 1297–1303. [PubMed: 20644199]

(73). Van der Auwera GA; Carneiro MO; Hartl C; Poplin R; Del Angel G; Levy-Moonshine A; Jordan T; Shakir K; Roazen D; Thibault J; Banks E; Garimella KV; Altshuler D; Gabriel S; DePristo MA From FastQ data to high confidence variant calls: the Genome Analysis Toolkit best practices pipeline. Curr. Protoc. Bioinf 2013, 43, 11.101–11.10.33.

(74). Cowell AN; Istvan ES; Lukens AK; Gomez-Lorenzo MG; Vanaerschot M; Sakata-Kato T; Flannery EL; Magistrado P; Owen E; Abraham M; LaMonte G; Painter HJ; Williams RM;

Franco V; Linares M; Arriaga I; Bopp S; Corey VC; Gnadig NF; Coburn-Flynn O; Reimer C; Gupta P; Murithi JM; Moura PA; Fuchs O; Sasaki E; Kim SW; Teng CH; Wang LT; Akidil A; Adjalley S; Willis PA; Siegel D; Tanaseichuk O; Zhong Y; Zhou Y; Llinas M; Ottilie S; Gamo FJ; Lee MCS; Goldberg DE; Fidock DA; Wirth DF; Winzeler EA Mapping the malaria parasite druggable genome by using in vitro evolution and chemogenomics. Science 2018, 359, 191–199. [PubMed: 29326268]

(75). Summers RL; Pasaje CFA; Pisco JP; Striepen J; Luth MR; Kumpornsin K; Carpenter EF; Munro JT; Lin; Plater A; Punekar AS; Shepherd AM; Shepherd SM; Vanaerschot M; Murithi JM; Rubiano K; Akidil A; Ottilie S; Mittal N; Dilmore AH; Won M; Mandt REK; McGowen K; Owen E; Walpole C; Llinas M; Lee MCS; Winzeler EA; Fidock DA; Gilbert IH; Wirth DF; Niles JC; Baragana B; Lukens AK Chemogenomics identifies acetyl-coenzyme A synthetase as a target for malaria treatment and prevention. Cell Chem. Biol 2022, 29, 191–201.e8. [PubMed: 34348113]

(76). Miles A; Iqbal Z; Vauterin P; Pearson R; Campino S; Theron M; Gould K; Mead D; Drury E; O'Brien J; Ruano Rubio V; MacInnis B; Mwangi J; Samarakoon U; Ranford-Cartwright L; Ferdig M; Hayton K; Su XZ; Wellems T; Rayner J; McVean G; Kwiatkowski D Indels, structural variation, and recombination drive genomic diversity in *Plasmodium falciparum*. Genome Res. 2016, 26, 1288–1299. [PubMed: 27531718]

(77). Navarrete-Perea J; Yu Q; Gygi SP; Paulo JA Streamlined Tandem Mass Tag (SL-TMT) Protocol: An Efficient Strategy for Quantitative (Phospho)proteome Profiling Using Tandem Mass Tag-Synchronous Precursor Selection-MS3. J. Proteome Res 2018, 17, 2226–2236. [PubMed: 29734811]

(78). Eng JK; Jahan TA; Hoopmann MR Comet: an open-source MS/MS sequence database search tool. Proteomics 2013, 13, 22–24. [PubMed: 23148064]

(79). Sanderson T; Rayner JC PhenoPlasm: a database of disruption phenotypes for malaria parasite genes. Wellcome Open Res. 2017, 2, 45. [PubMed: 28748223]

(80). Aurrecoechea C; Brestelli J; Brunk BP; Dommer J; Fischer S; Gajria B; Gao X; Gingle A; Grant G; Harb OS; Heiges M; Innamorato F; Iodice J; Kissinger JC; Kraemer E; Li W; Miller JA; Nayak V; Pennington C; Pinney DF; Roos DS; Ross C; Stoeckert CJ Jr.; Treatman C; Wang H PlasmoDB: a functional genomic database for malaria parasites. Nucleic Acids Res. 2009, 37, D539–543. [PubMed: 18957442]

(81). Supek F; Bosnjak M; Skunca N; Smuc T REVIGO summarizes and visualizes long lists of gene ontology terms. PLoS One 2011, 6, No. e21800. [PubMed: 21789182]

(82). Shannon P; Markiel A; Ozier O; Baliga NS; Wang JT; Ramage D; Amin N; Schwikowski B; Ideker T Cytoscape: a software environment for integrated models of biomolecular interaction networks. Genome Res. 2003, 13, 2498–2504. [PubMed: 14597658]

(83). Szklarczyk D; Gable AL; Nastou KC; Lyon D; Kirsch R; Pyysalo S; Doncheva NT; Legeay M; Fang T; Bork P; Jensen LJ; von Mering C The STRING database in 2021: customizable protein-protein networks, and functional characterization of user-uploaded gene/measurement sets. Nucleic Acids Res. 2021, 49, D605–D612. [PubMed: 33237311]
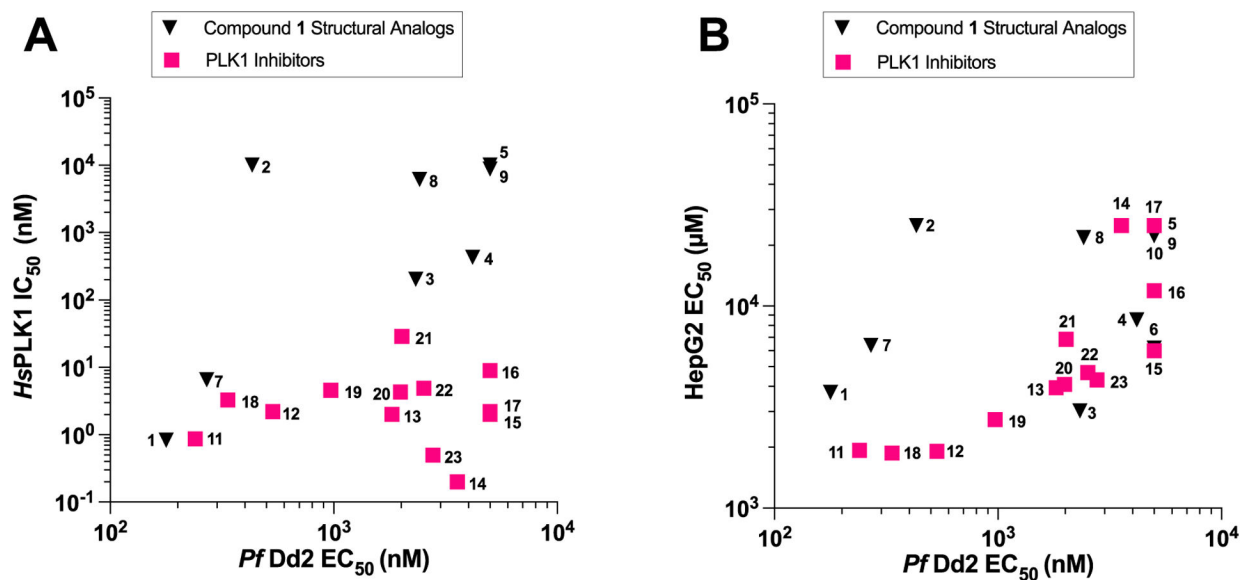
Figure 1.

Antiplasmodial potency not correlated with human PLK1 inhibition. (A) Average Dd2 EC_{50} values are plotted against human PLK1 IC_{50} values (PLK1 Inhibitors $r^2 = 3.089 \times 10^{-5}$, $p = 0.9856$; compound **1** structural analogues $r^2 = 0.1578$, $p = 0.3299$). (B) HepG2 EC_{50} values plotted against Dd2 EC_{50} values (PLK1 inhibitors: $r^2 = 0.4635$, $p = 0.0104$; compound **1** structural analogues: $r^2 = 0.1144$, $p = 0.3391$).
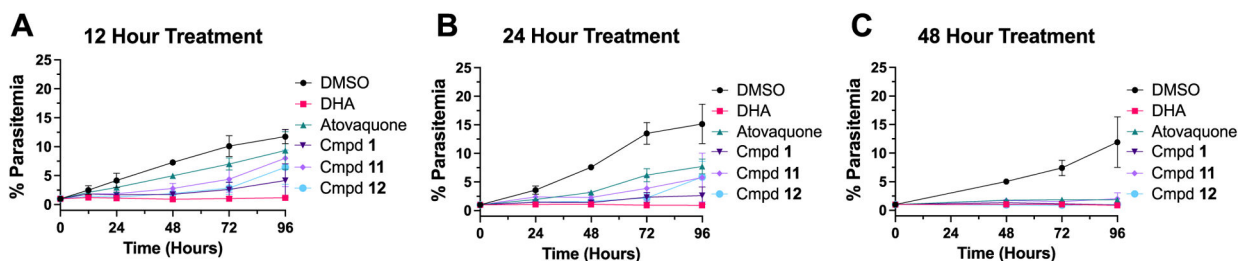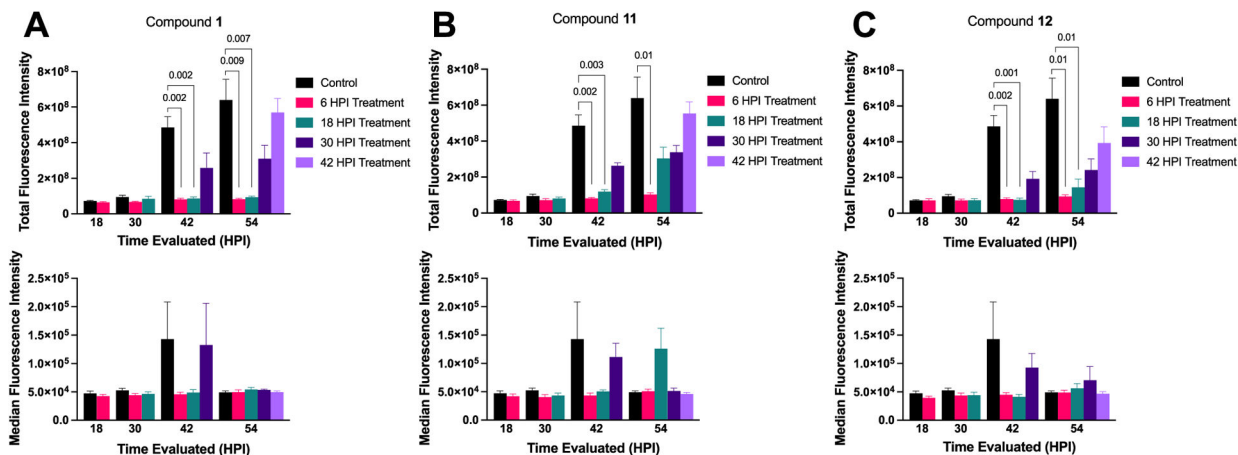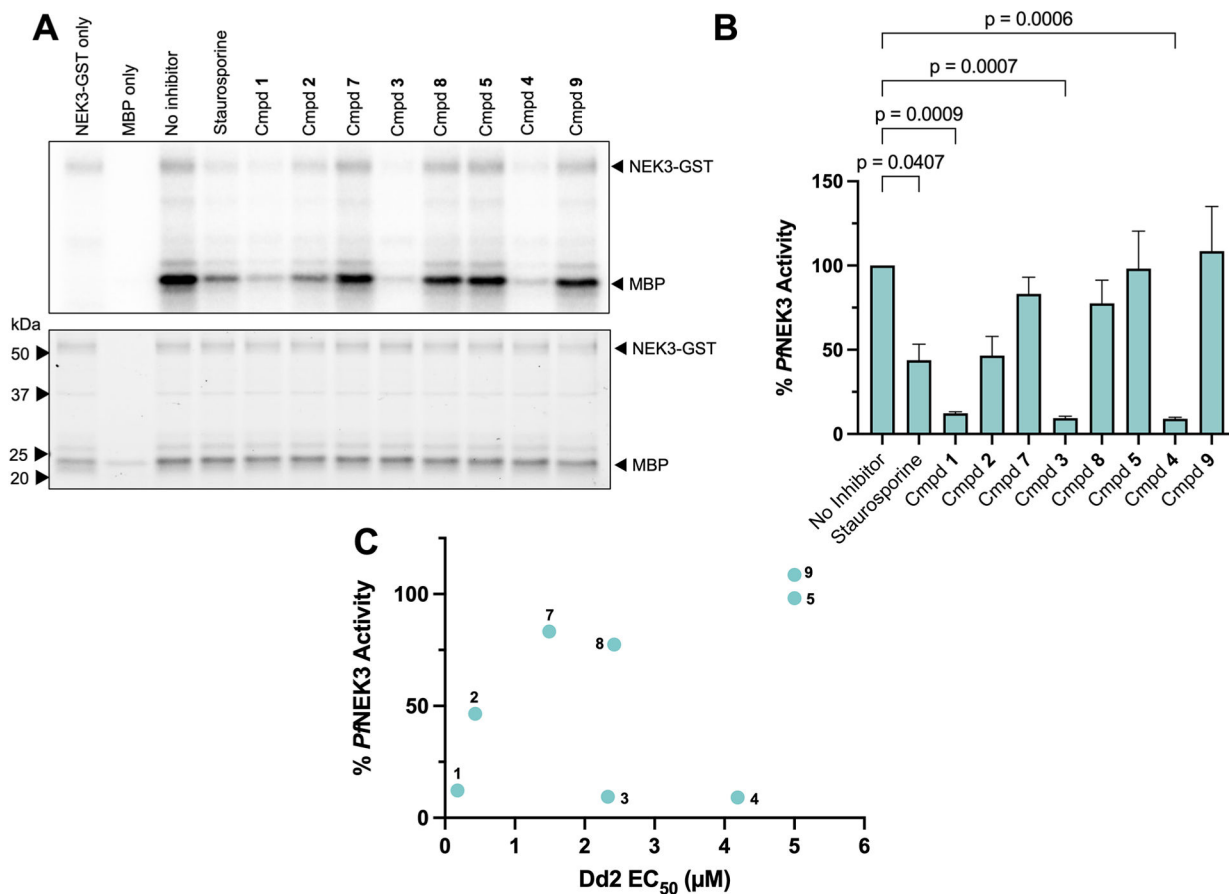
Figure 2.

PLK1 inhibitors display similar killing profile. Dd2 parasites were treated at 1% parasitemia with $10 \times EC_{50}$ of compound **1, 11, 12**, or controls for 12 h (A), 24 h (B), or 48 h (C) prior to compound wash off. Samples were collected every 24 h and treated with nucleic acid stain SYBR Green I and MitoTracker Deep Red FM. Double-positive cells were considered viable. DHA and atovaquone served as fast-acting and slow-acting controls, respectively. The results displayed are the average of three biological replicates ± SEM.

Figure 3.

Blood stage specificity of PLK1 inhibitors. Synchronized Dd2 parasites were treated at set timepoints and evaluated every 12 h throughout the life cycle until post-reinvasion. Changes in DNA content were assessed in YOYO-1-stained parasites with flow cytometry. For YOYO-1 positive populations, the total DNA content (top) as well as median DNA content per cell (bottom) for compound **1** (A), compound **11** (B), and compound **12** (C) are evaluated. Graphs depict averages of four biological replicates $\pm$ SEM. Treatment conditions were each compared to the control with *t*-test with the Holm–Šídák method for multiple corrections. *P*-values less than 0.05 are shown.

Figure 4.

*Pf*NEK3 inhibition not the sole predictor of antiplasmodial activity. (A) Inhibition of *Pf*NEK3 following incubation with 1 μM PLK inhibitors. Top: Autoradiogram. Bottom: TCE gel image for protein quantification. A 1 μM pan-kinase inhibitor staurosporine serves as a control. Gel representative of three replicates. (B) Quantification of kinase activity. Autoradiogram band intensity normalized to protein concentration by the TCE gel band. Activity normalized to the no-inhibitor control (100% activity). Data shown represents averages ± SEM of three replicates. Significance of treatments compared to the no-inhibitor control determined by one-way analysis of variance (ANOVA). (C) Relationship between Dd2 EC 50 and *Pf*NEK3 activity remaining after 1 μM treatment ($r^2 = 0.2117$, $p = 0.25$).
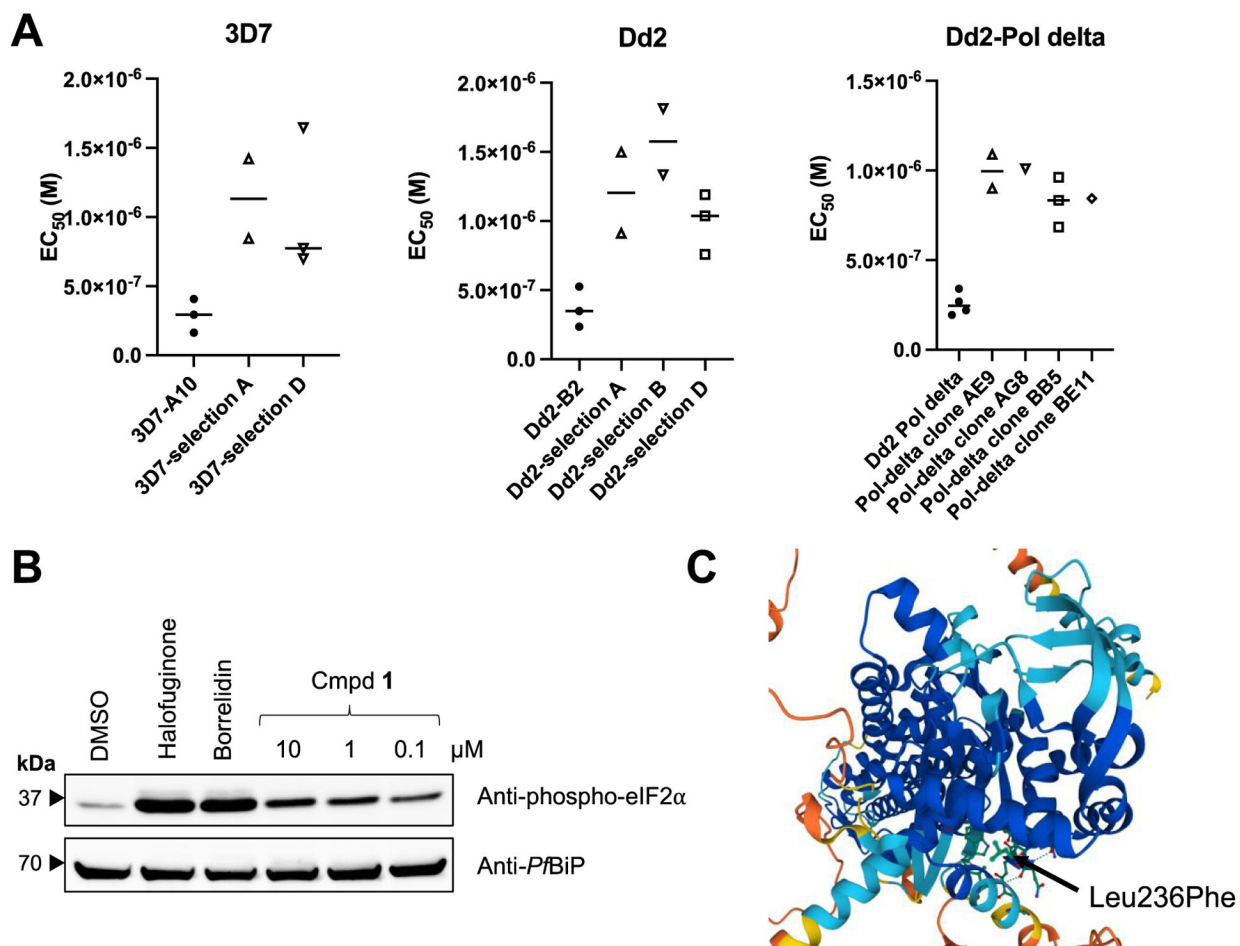
Figure 5.
Compound **1** induces eIF2a-mediated stress response. (A) Parasites with resistance to compound **1** obtained from *P. falciparum* three strains. (B) Western blot reveals that Dd2 parasites treated with Compound **1** exhibit increased phospho-eIF2a phosphorylation compared to the vehicle control (dimethyl sulfoxide (DMSO)), though not as much as the positive phosphorylation controls, borrelidin and halofuginone. Blot is representative of three biological replicates. (C) Missense mutation is located at the conserved residue in MRS[api] (UniProt ID: Q8IJ60). Predicted structure derived from AlphaFold (www.alphafold.ebi.ac.uk).
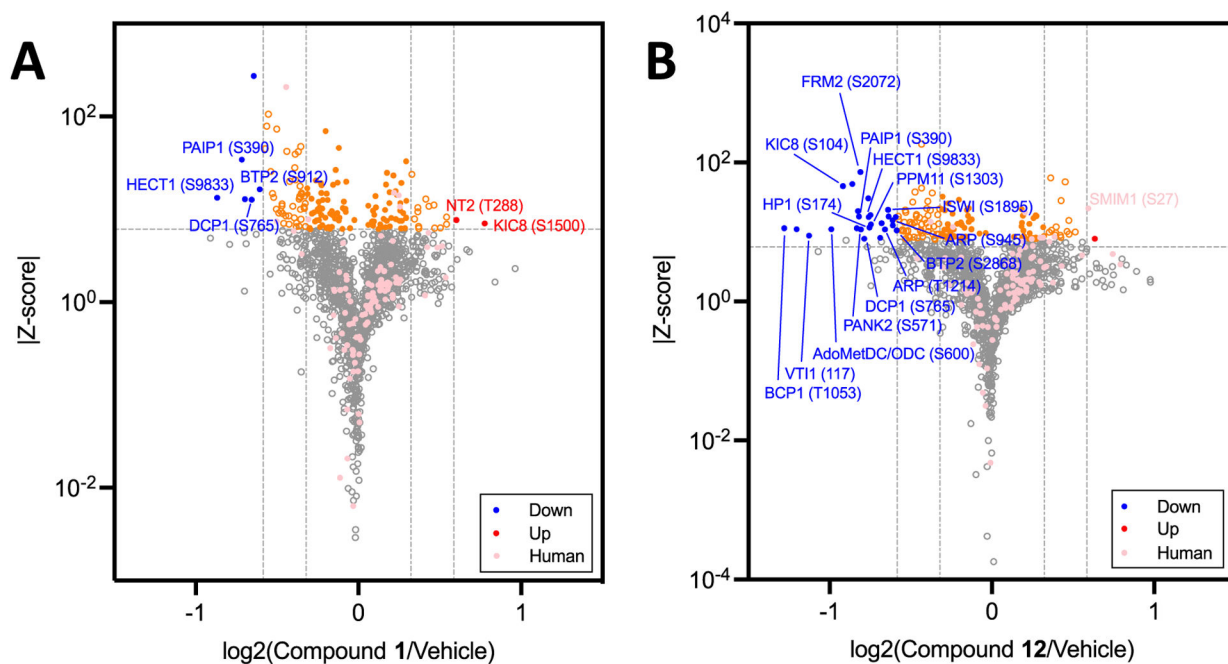
Figure 6.

Differentially expressed phosphosites upon exposure to compound **1** (A) and compound **12** (B) of the top-ranked most downregulated (log 2(fc) < −0.585) motifs per treatment. Dashed lines on volcano plots represent cutoff values of the top 10% of the absolute values of the |Z-score| and |log 2(fc)| > 0.585, and dotted lines represent |log 2(fc)| > 0.322.
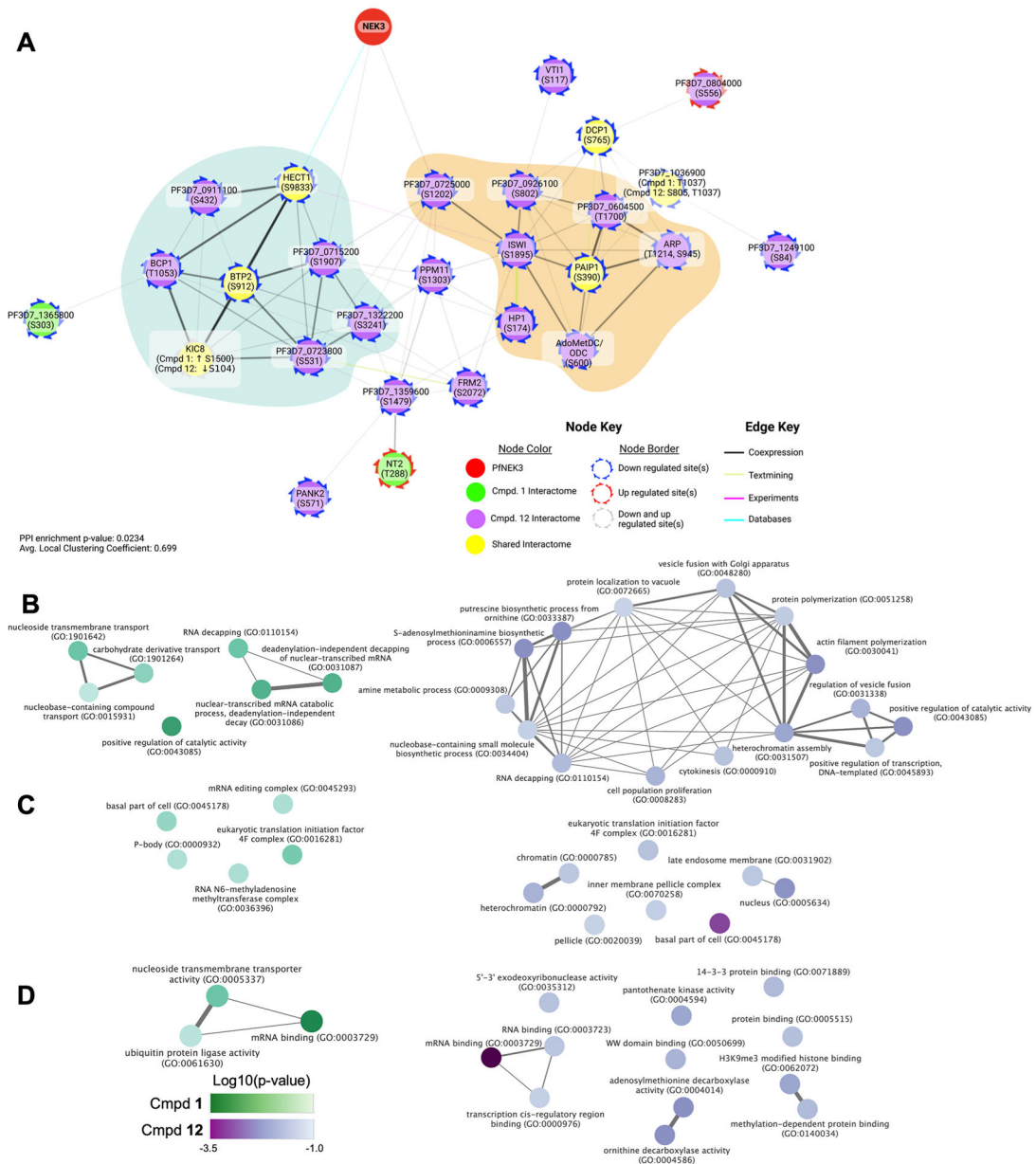
Figure 7.
Interactome of compounds **1** and **12** and resulting GO enrichment analysis. (A) STRING network of proteins possessing the top differential (|log 2(*fc*)| > 0.585) phosphosites with *Pf* NEK3. Color represents the interactome source (compound **1**, compound **12**, shared), border color represents the direction of deregulation. Edge color represents strongest contributing source, and edge thickness represents the overall edge score. (B–D) Shared and distinct GO enrichment for compound **1** (green) and compound **12** (purple) for the biological process (B), cellular component (C), and molecular function (D). Color intensity reflects log 10 (enrichment *p*-value), and edge indicates similarity between terms.

Table 1.

Antiplasmodial and Kinase Activities of Compound 1 Structural Analogues

Compound 1

Compound 2

Compound 3

Compound 4

Compound 5

Compound 6

Compound 7

Compound 8

Compound 9

Compound 10

ID	antiplasmodial activity			cytotoxicity		kinase activity
	Pf Dd2 EC$_{50}$ (nM)	*Pf* 3D7 EC$_{50}$ (nM)	RI[a]	HepG2 EC$_{50}$ (nM)	SI[b]	PLK1 IC$_{50}$ (nM)
BI-2536 (1)	178 ± 12	135 ± 35	1.3	3730 ± 520	21	0.83
compound 2	432 ± 47	347 ± 52	1.2	>25,000	> 58	>10,000
compound 3	2330 ± 160	1530 ± 250	1.5	3030 ± 200	1.0	204
compound 4	4190 ± 260	3250 ± 550	1.3	8550 ± 720	2.0	430
compound 5	>5000	nt	-	>25,000	-	>10,000
compound 6	>5000	nt	-	6200 ± 470	<1.0	nt
compound 7	1490 ± 260	1540 ± 350	0.97	6390 ± 130	4.0	270
compound 8	2420 ± 440	2350 ± 650	1.0	21,800 ± 700	9.0	6200
compound 9	>5000	nt	-	>25,000	-	8800
compound 10	>5000	nt	-	22,300 ± 1290	<4.0	nt

[a] Resistance Index (RI) = Dd2 EC$_{50}$/3D7 EC$_{50}$.

[b] Selectivity Index (SI) = HepG2 EC$_{50}$/Dd2 EC$_{50}$.

Values shown are the average EC50 ± standard error of the mean (SEM) from at least three biological replicates. Human PLK1 IC50 values were obtained from prior publication or from Selleck Chemicals.[15,16]

c
nt = not tested.

Table 2.

Antiplasmodial and Kinase Activities of PLK1 Inhibitors

Compound 11 Compound 12 Compound 13 Compound 14 Compound 15

Compound 16 Compound 17

Compound 18, R = ... Compound 19, R = ...

Compound 20, R = -Br
Compound 21, R = -F
Compound 22, R = -CN
Compound 23, R = -CF3

ID	antiplasmodial activity			cytotoxicity		kinase activity
	Pf Dd2 EC$_{50}$ (nM)	Pf 3D7 EC$_{50}$ (nM)	RI[a]	HepG2 EC$_{50}$ (nM)	SI[b]	PLK1 IC$_{50}$ (nM)
BI-6727 (**11**)	230 ± 14	284 ± 52	0.81	1930 ± 460	8.0	0.87
GSK461364 (**12**)	533 ± 78	1410 ± 77	0.34	1910 ± 210	4.0	2.2
MLN0905 (**13**)	1820 ± 260	nt	-	3940 ± 110	2.0	2.0
SBE 13 (**14**)	3570 ± 130	nt	-	>25,000	>7.0	0.20
NMS-P937 (**15**)	>5000	nt	-	6010 ± 79	<1.0	2.0
ON-01910 (**16**)	>5000	nt	-	11,900 ± 42	<2.0	9.0
GW843682 (**17**)	>5000	nt	-	>25,000	-	2.2
Compound **18**	336 ± 34	315 ± 11	1.1	1870 ± 190	6.0	3.3
Compound **19**	971 ± 58	759 ± 96	1.3	2740 ± 310	2.0	4.6
Compound **20**	1990 ± 34	1860 ± 330	1.1	4090 ± 440	2.0	4.3
Compound **21**	2020 ± 150	2020 ± 340	1	6840 ± 210	3.0	29
Compound **22**	2530 ± 130	nt	-	4690 ± 690	2.0	4.9
Compound **23**	2780 ± 290	nt	-	4300 ± 450	2.0	<0.50

[a] Resistance Index (RI) = Dd2 EC50/3D7 EC50.

[b] $_{50}$ Selectivity Index (SI) = HepG2 EC$_{50}$/Dd2 EC$_{50}$.

[c] $_{50}$ nt = not tested.

Values shown are the average EC$_{50}$ ± SEM from at least three biological replicates. Human PLK1 IC$_{50}$ values were obtained from prior publication or from Selleck Chemicals.[15,16]

Table 3.

PLK1 Inhibitors Show *Pf*NEK3 Inhibition *In Vitro*[a]

							% activity remaining at 2.5 μM in plasmodial kinases					
compound	ARK1	ARK3	CDPK2	CDPK5	GSK3	NEK1	NEK3	PK5	PK6	PK9	PKB
1	100.0	100.0	80.6	100.0	99.4	94.5	4.7 (86 ± 11)	100.0	94.6	97.2	100.0
2	53.4	73.5	100.0	100.0	100.0	93.3	39.6 (1480 ± 150)	100.0	94.8	100.0	64.2
11	100.0	83.6	100.0	100.0	100.0	93.8	11.1 (130 ± 20)	100.0	67.3	100.0	49.3
12	99.5	96.2	100.0	100.0	100.0	100.0	9.7 (19 ± 30)	100.0	100.0	100.0	100.0
18	73.9	84.6	24.0 (390 ± 50)	88.1	100.0	96.4	15.4 (630 ± 120)	100.0	78.9	78.7	12.3 (250 ± 60)
19	77.9	83.6	36.1 (780 ± 90)	100.0	100.0	90.1	18.5 (1820 ± 210)	100.0	91.0	85.7	14.8 (790 ± 140)

[a]Values are % activity remaining.

Values in parentheses are IC50 values in nM ± SD.